

BISON Simulated and Experimental Fission Product Release Comparisons from Re-Irradiated AGR-3/4 Compacts During High-Temperature Heating Tests

SEPTEMBER 2024

William F. Skerjanc
Jacob A. Hirschhorn
Javier Ortensi

Idaho National Laboratory



DISCLAIMER

This information was prepared as an account of work sponsored by an agency of the U.S. Government. Neither the U.S. Government nor any agency thereof, nor any of their employees, makes any warranty, expressed or implied, or assumes any legal liability or responsibility for the accuracy, completeness, or usefulness, of any information, apparatus, product, or process disclosed, or represents that its use would not infringe privately owned rights. References herein to any specific commercial product, process, or service by trade name, trade mark, manufacturer, or otherwise, does not necessarily constitute or imply its endorsement, recommendation, or favoring by the U.S. Government or any agency thereof. The views and opinions of authors expressed herein do not necessarily state or reflect those of the U.S. Government or any agency thereof.

BISON Simulated and Experimental Fission Product Release Comparisons from Re-Irradiated AGR-3/4 Compacts During High-Temperature Heating Tests

**William F. Skerjanc
Jacob A. Hirschhorn
Javier Ortensi
Idaho National Laboratory**

September 2024

**Idaho National Laboratory
Advanced Reactor Technologies
Idaho Falls, Idaho 83415**

<http://www.art.inl.gov>

**Prepared for the
U.S. Department of Energy
Office of Nuclear Energy
Under DOE Idaho Operations Office
Contract DE-AC07-05ID14517**

Page intentionally left blank

INL ART Program

**BISON Simulated and Experimental Fission Product
Release Comparisons from Re-Irradiated AGR-3/4
Compacts During High-Temperature Heating Tests**

INL/RPT-24-80652

September 2024

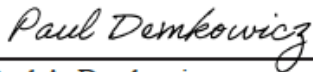


Adriaan A. Riet
AGR PIE Analyst

September 12, 2024

Date

Approved by:



Paul A. Demkowicz
AGR Fuels Technical Director

9/17/2024

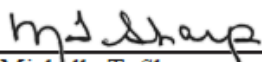
Date



Travis R. Mitchell
ART Project Manager

9/12/2024

Date



Michelle T. Sharp
INL Quality Assurance

9/17/2024

Date

Page intentionally left blank

ABSTRACT

The fuel performance modeling code BISON was used to predict the release of fission products ^{131}I , ^{133}Xe , and ^{85}Kr from four re-irradiated AGR-3/4 fuel compacts containing tristructural isotropic (TRISO)-coated particles during high-temperature isothermal heating tests. The AGR-3/4 fuel compacts were irradiated in the Advanced Test Reactor (ATR) as part of the third and fourth series of planned experiments to support the Advanced Gas Reactor (AGR) Program. They were subsequently stored and re-irradiated in the Neutron Radiography (NRAD) reactor for approximately five days and then stored for another five to eight days before being subjected to isothermal heating tests in the Fuel Accident Condition Simulation (FACS furnace) for 200 to 300 hours at temperatures between 1000°C and 1600°C to evaluate fission product release at elevated temperatures.

New nuclide-specific fission product source term models for the three nuclides of interest were developed using the reactor multiphysics code Griffin and were implemented into BISON to support this work. The new source term models were incorporated into coupled compact- and particle-scale BISON simulations, which predict spatially- and temporally resolved radionuclide generation, radioactive decay, transport, and release throughout the entire irradiation history, including the initial ATR irradiation, NRAD re-irradiations, FACS heating tests, and intermediate periods spent in storage.

The experimentally measured fission product release from the heating tests was compared to modeling release predictions calculated by BISON to evaluate how well the code compares to experimental results. Overall, the experimentally measured and BISON predicted comparative release results varied but generally agreed to within five particle equivalents. The comparison resulted in some general observations which should be considered to help refine future models and reduce uncertainties associated with both the measurements and the predictions. This includes developing new uranium oxycarbide (UCO) specific kernel diffusivities for the three isotopes examined to more accurately reflect the material properties of the fuel form. Deriving new diffusivities will aid in producing a more informed BISON model.

Page intentionally left blank

CONTENTS

ABSTRACT.....	vii
ACRONYMS.....	xiv
1. INTRODUCTION.....	1
1.1. AGR Fuel Development and Qualification Program.....	1
1.2. BISON.....	2
2. AGR-3/4 EXPERIMENT.....	3
2.1. Fuel Characteristics.....	3
2.2. AGR-3/4 Description.....	5
2.3. AGR-3/4 Irradiation.....	7
2.4. Compact Re-irradiation.....	8
2.5. Heating Tests.....	8
3. MODELING INPUT AND METHODOLOGY.....	10
3.1. Input Parameters.....	10
3.2. AGR Irradiation Conditions.....	11
3.3. NRAD Irradiation Conditions.....	12
3.4. FACS Heating Test Conditions.....	12
3.5. Fission Product Accounting.....	13
3.5.1 Source term development.....	15
3.5.2 Fission product tracking.....	21
3.5.3 Multiscale BISON simulations.....	23
3.5.4 Application to Compact 3-1.....	25
3.6 Fission Product Transport.....	26
4. COMPARITIVE RELEASE RESULTS.....	28
4.1 FACS Heating Test of Compact 3-1 at 1600°C.....	30
4.2 FACS Heating Test of Compact 10-1 at 1400°C.....	31
4.3 FACS Heating Test of Compact 8-1 at 1200°C.....	32
4.4 FACS Heating Test of Compact 4-3 at 1000°C.....	34
4.5 Iodine Release.....	34
4.6 Xenon Release.....	36
4.7 Krypton Release.....	37
5. DISCUSION OF RESULTS.....	40
6. CONCLUSION.....	43
7. REFERENCES.....	44

FIGURES

Figure 1. Monte Carlo methodology for calculating TRISO particle failure probability in BISON.	2
Figure 2. Typical TRISO-coated fuel particle geometry.	4
Figure 3. Schematic of an AGR-3/4 compact with DTF fuel particles (red) along the cylindrical axis of symmetry.	5
Figure 4. ATR core cross-section displaying the NEFT position.	5
Figure 5. Axial schematic of the AGR-3/4 capsules.	6
Figure 6. Radial schematic of the AGR-3/4 capsule.	7
Figure 7. Cross section view of the NRAD TRIGA reactor core configuration.	8
Figure 8. Graphic of the FACS furnace used to conduct heating tests.	9
Figure 9. Evolution of the FACS furnace heating tests temperatures for selected re-irradiated AGR-3/4 compacts.	13
Figure 10. Capsule 5 MCNP spectrum for various ATR fuel cycles versus approximated flux with a 3.0 cm graphite holder.	14
Figure 11. Simplified cross-sectional representation of AGR-2 used for Griffin depletion and transmutation analyses, which includes a homogenized TRISO compact (center) and borated graphite holder (periphery).	15
Figure 12. Examples of supplied and calculated linear powers (top left), supplied compact average temperature (top right), and calculated neutron flux (bottom center) from Griffin decay and transmutation simulations.	16
Figure 13. Relative fission yields of eight fuel nuclides predicted using the DRAGON–Griffin workflow (lines) compared to EOI MCNP/ORIGEN predictions from AGR-2 physics analyses (points). The same data are plotted on log (left) and linear (right) scales.	17
Figure 14. Evolution of the three nuclides of interest predicted by Griffin compared to EOI predictions from MCNP/ORIGEN. Other key isotopes associated with each element and elemental inventories are also included. Note that not all isotopes associated with each element are shown. The xenon predictions are shown on a log scale to more clearly illustrate the ^{133}Xe results.	18
Figure 15. Evolution of the four additional elements and associated isotopes, for which MCNP/ORIGEN predictions and AGR-2 PIE measurements are available for comparison.	19
Figure 16. Evolution of selected xenon isotopes, including ^{133}Xe , which was assumed to be stable in this simulation to isolate its production for development into a nuclide-specific source term for BISON. Note that ^{133}Xe still tends to plateau due to neutron capture.	20
Figure 17. Evolution of selected xenon isotopes using Griffin, inventory-dependent fission yield correlations developed from Griffin results, and the existing BISON source term model. As before, ^{133}Xe was assumed to be stable to isolate its production term.	21
Figure 18. Evolution of selected krypton and iodine isotopes using Griffin and the inventory-dependent fission yield correlations developed from Griffin results.	22

Figure 19. Final comparisons between Griffin and BISON predictions for the three nuclides of interest. The Griffin predictions include the effects of decay for all three nuclides. The BISON predictions were obtained using the new inventory-dependent fission yield correlations and also include the effects of decay.	23
Figure 20. Combined thermal and irradiation histories constructed to simulate the initial AGR-3/4 irradiation, NRAD re-irradiation, and FACS testing for Compact 3-1 in BISON. Portions of the storage between the initial irradiation and NRAD re-irradiation are omitted to more clearly illustrate features of interest.	26
Figure 21. Diffusivities for iodine, xenon, and krypton as a function of temperature.	28
Figure 22. Summary of total particle equivalent release at the end of FACS heating tests. Note that the compacts are presented from left to right in decreasing FACS heating test temperature. Results from Compact 10-1 include a failed driver fuel particle 18 hours into FACS testing.	30
Figure 23. Time-dependent measured release from Compact 3-1 at 1600°C. The same data are plotted on linear (left) and log (right) scales.	30
Figure 24. Time-dependent measured release from Compact 10-1 at 1400°C. The same data are plotted on linear (left) and log (right) scales.	32
Figure 25. Time-dependent measured release from Compact 8-1 at 1200°C. The same data are plotted on linear (left) and log (right) scales.	33
Figure 26. Time-dependent measured release from Compact 4-3 at 1000°C. The same data are plotted on linear (left) and log (right) scales.	34
Figure 27. Time-dependent measured release of ¹³¹ I. The same data are plotted on linear (left) and log (right) scales.	35
Figure 28. ¹³¹ I release as a fraction of inventory produced in DTF particles.	35
Figure 29. ¹³¹ I release from Compacts 3-1 and 10-1 early in the FACS heating test.	36
Figure 30. Time-dependent measured release of ¹³³ Xe. The same data are plotted on linear (left) and log (right) scales.	37
Figure 31. ¹³³ Xe release as a fraction of inventory produced in DTF particles.	37
Figure 32. As-run neutronic calculated and BISON predicted ⁸⁵ Kr inventory post ATR irradiation (EOI plus one day).	38
Figure 33. Time-dependent measured release of ⁸⁵ Kr. The same data are plotted on linear (left) and log (right) scales.	39
Figure 34. ⁸⁵ Kr release as a fraction of inventory produced in DTF particles.	39
Figure 35. Cut-away view a typical temperature (°C) contour plot of an AGR-3/4 capsule (Hawkes 2016).	42

TABLES

Table 1. Primary functions of particle fuel components.	4
Table 2. FACS furnace condensation plate collection efficiencies for ¹³¹ I.	10
Table 3. Compact evolution from ATR irradiation to FACS heat testing.	10

Table 4. Parameters used to model the AGR-3/4 experiment.....	11
Table 5. Selected AGR-3/4 compacts EOI TAVA temperatures, accumulated fluence, and burnup.....	12
Table 6. Re-irradiation duration for select compacts in NRAD.....	12
Table 7. Coefficients of the nuclide-specific fission yields fit to inventories. The correlations have the form $\gamma = (aNi^2 + bNi + c)/1 \times 1030$, where γ is the fission yield in mol/fission and Ni is the nuclide number density in mol/m ³	22
Table 8. Key behavioral models, material properties, and the BISON classes used to model them at the compact scale.	24
Table 9. Key behavioral models and material properties, as well as the BISON classes used to model them at the particle scale.....	24
Table 10. Effective diffusivity pre-factors and activation energies used in BISON for iodine, xenon, and krypton.	27
Table 11. Total release from Compact 3-1 at 1600°C.....	31
Table 12. Total release from Compact 10-1 at 1400°C.	32
Table 13. Total release from Compact 8-1 at 1200°C.	33
Table 14. Total release from Compact 4-3 at 1000°C.	34
Table 15. BISON predicted produced and retained ⁸⁵ Kr inventory at the EOI in the ATR.	38
Table 16. Physics calculated inventories versus decay-corrected inventories and the resulting measured releases for Compact 3-1.....	41

Page intentionally left blank

ACRONYMS

AGR	Advanced Gas Reactor
ART	Advance Reactor Technologies
ATR	Advanced Test Reactor
CEGA	Combustion Engineering/General Atomics
DTF	designed-to-fail
DTL	decay-transmutation library
EFPD	effective full power days
EOI	end-of-irradiation
FACS	Fuel Accident Condition Simulator
FIMA	fissions per initial heavy metal atom
HFEF	Hot Fuels Examination Facility
HTGR	high-temperature gas-cooled reactor
IAEA	International Atomic Energy Agency
INL	Idaho National Laboratory
IPyC	inner pyrolytic carbon
LEU	low enriched uranium
MCNP	Monte Carlo N-Particle
MOOSE	Multiphysics Object-Oriented Simulation Environment
NDMAS	Nuclear Data Management and Analysis System
NEFT	northeast flux trap
NRAD	Neutron Radiography
OPyC	outer pyrolytic carbon
ORIGEN	Oak Ridge Isotope Generation
PALM	power axial locator mechanism
PARFUME	PARticle FUEl ModEl
PIE	post-irradiation examination
SiC	silicon carbide
TAVA	time-average volume average
TRIGA	Training, Research, Isotopes, General Atomics
TRISO	tristructural isotropic
UCO	uranium oxycarbide

Page intentionally left blank

BISON Simulated and Experimental Fission Product Release Comparisons from Re-Irradiated AGR-3/4 Compacts During High-Temperature Heating Tests

1. INTRODUCTION

Several fuel and material irradiation experiments have been completed during the DOE Advanced Reactor Technologies (ART) Advanced Gas Reactor (AGR) Fuel Development and Qualification Program. These experiments support the development and qualification of tristructural isotropic (TRISO)-coated particle fuel for use in high-temperature gas-cooled reactors (HTGRs). The goals of these experiments are to provide irradiation performance data to support fuel process development, qualify fuel for normal operating conditions, support the development and validation of fuel performance and fission product transport models and codes, and provide irradiated fuel and materials for post-irradiation examination (PIE) and safety testing (Mitchell and Demkowicz 2022). AGR-3/4 combined the third and fourth in this series of experiments to test TRISO-coated, low-enriched uranium (LEU) oxycarbide (UCO) fuel.

This report documents comparisons between the fission product release observed during heating tests of selected re-irradiated AGR-3/4 fuel compacts and the corresponding fission product release fractions predicted by the finite element-based code BISON (Williamson, et al. 2021) for the isotopes ^{131}I , ^{133}Xe , and ^{85}Kr . The AGR-3/4 experiment was irradiated from December 2011 to April 2014 in the Advanced Test Reactor (ATR) over a total of 10 ATR cycles, including seven normal cycles, one low-power cycle, one unplanned outage cycle, and one power axial locator mechanism (PALM) cycle for a total of 369.1 effective full power days (EFPD) (Collin 2016). The modeling only covers the seven normal power cycles since the experiment test train was moved to the ATR canal during the unplanned outage and the PALM cycles and given that no burnup was being accumulated during the low-power cycle.

More than five years after the ATR irradiation, select compacts were then re-irradiated in the Neutron Radiography (NRAD) Reactor at the INL Hot Fuels Examination Facility (HFEF) to produce short-lived fission products. Following re-irradiation, the compacts were transferred to the Fuel Accident Condition Simulator (FACS) furnace, also located at HFEF, and were subjected to isothermal heating tests. Heating tests were performed for a range of postulated reactor accident conditions (Stempien, et al. 2021) and the experimental fission product release fractions were compared to the predicted values from the fuel performance code BISON. Previous heating test comparisons were performed using the PARTicle FUEL Model (PARFUME) (Miller et al. 2023) TRISO fuel performance code and PIE data from the AGR-1 (Collin 2014) and AGR-2 (Skerjanc 2020) experiments. In addition, heating tests of AGR-3/4 as-irradiated compacts were completed and the release predictions from PARFUME/BISON were compared to PIE release fraction measurements of silver, cesium, and strontium (Skerjanc 2023).

Details associated with these calculations along with the experimental measurement data are provided in the remainder of this document.

1.1. AGR Fuel Development and Qualification Program

The U.S. Department of Energy AGR Fuel Development and Qualification program was established to qualify TRISO-coated fuel for use in HTGRs. The primary goal of the program is to provide a baseline fuel qualification data set in support of the licensing and operation of an HTGR (Mitchell and Demkowicz 2022).

Seven fuel and material irradiation experiments were planned for the AGR program. The overall objectives of these experiments are as follows (Mitchell and Demkowicz 2022):

- Develop fuel fabrication capabilities
- Perform fuels and materials irradiation
- Perform safety testing and PIE
- Improve fuel performance modeling
- Evaluate fission product transport and source term determination.

1.2. BISON

BISON (Williamson, et al. 2021) is a nuclear fuel performance application built using the Multiphysics Object-Oriented Simulation Environment (MOOSE) framework (Giudicelli, et al. 2024) developed at INL that is capable of modeling multiple fuel forms in a wide variety of dimensions and geometries. BISON/MOOSE solves coupled nonlinear partial differential equations, including heat conduction, mechanics, and fission product species transport in a fully implicit manner. More detailed descriptions of the BISON fuel performance code as it relates to TRISO fuel modeling can be found in “BISON TRISO Modeling Advancements and Validation to AGR-1 Data” (Hales et al. 2020), “Numerical Evaluation of AGR-2 Fission Product Release” (Hales et al. 2021a), and “TRISO particle fuel performance and failure analysis with BISON” (Jiang et al. 2021). The Monte Carlo methodology used in BISON to calculate the failure probability of a batch of fuel particles is summarized in Figure 1 (Jiang et al. 2021). Recently, a more efficient statistical failure analysis, similar to the “fast” integration methodology in PARFUME, has been added to BISON (Jiang et al. 2022).

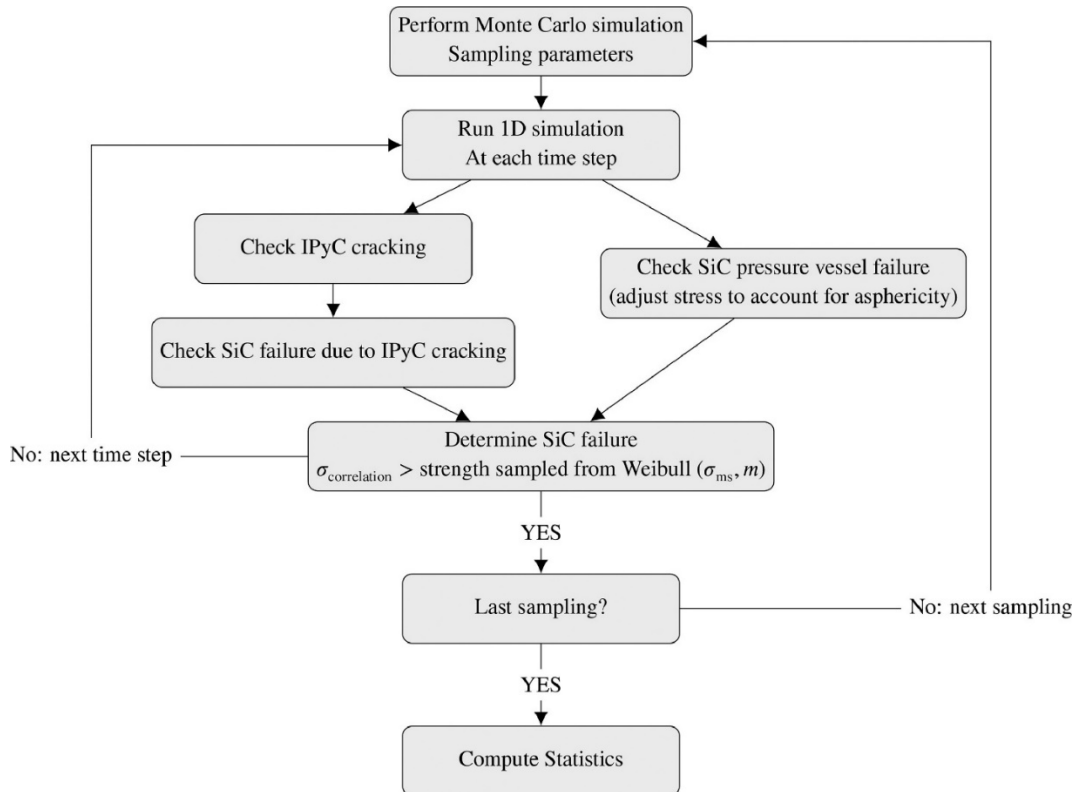


Figure 1. Monte Carlo methodology for calculating TRISO particle failure probability in BISON.

BISON has the capability to incorporate different irradiation conditions and run either very small analyses with a single processor or very large analyses with multiple processors on a supercomputer. For TRISO fuel, BISON supports spherically symmetric models, axisymmetric models, and full 3D models. Thermomechanical and irradiation behavior models for each material layer include elasticity, thermal and irradiation creep, irradiation-induced dimension change, thermal expansion, thermal conductivity, and more.

Fission product generation, diffusion, and release can also be modeled for TRISO particles with UO₂, UCO, or uranium nitride kernels. In addition, BISON can perform statistical failure analyses for large populations of fuel particles, a capability that enables evaluation of failure due to multidimensional phenomena by analyzing thousands of particles. This enables realistic calculations of the fission product release from the many particles in a TRISO-fueled reactor.

2. AGR-3/4 EXPERIMENT

As defined in the technical program plan for the INL ART/AGR fuel program (Mitchell and Demkowicz 2022), the AGR-3/4 experiment objectives are as follows:

1. Irradiate fuel containing UCO designed-to-fail (DTF) fuel particles that will provide a known source of fission products for subsequent transport through compact matrix and structural graphite materials.
2. Assess the effects of sweep gas impurities (such as CO, H₂O, and H₂) typically found in the primary coolant circuit of HTGRs, on fuel performance and subsequent fission product transport.
3. Provide irradiated fuel and material samples for PIE and post-irradiation heating tests.
4. Support the refinement of fuel performance and fission product transport models with online, PIE, and post-irradiation heating test data.

2.1. Fuel Characteristics

Fuel for AGR-3/4 contained conventional driver fuel particles similar to the baseline particles used in the AGR-1 experiment (Barnes 2006a) and DTF fuel particles whose kernels were identical to the driver fuel kernels with a single coating layer that was DTF under irradiation, leaving fission products to migrate through the surrounding materials (Barnes 2006b) (Marshall 2011).

- Driver fuel consisted of TRISO-coated particles that were slightly less than 1 mm in diameter. Each particle had a central reference kernel that contains fuel material, a porous carbon buffer layer, an inner pyrolytic carbon (IPyC) layer, a silicon carbide (SiC) barrier coating, and an outer pyrolytic carbon (OPyC) layer as depicted in Figure 2. Each layer's function is described in Table 1.
- DTF fuel consisted of reference kernels with a 20-μm-thick pyrolytic carbon seal coating. This coating was DTF early in the irradiation and provided a known source of fission products.

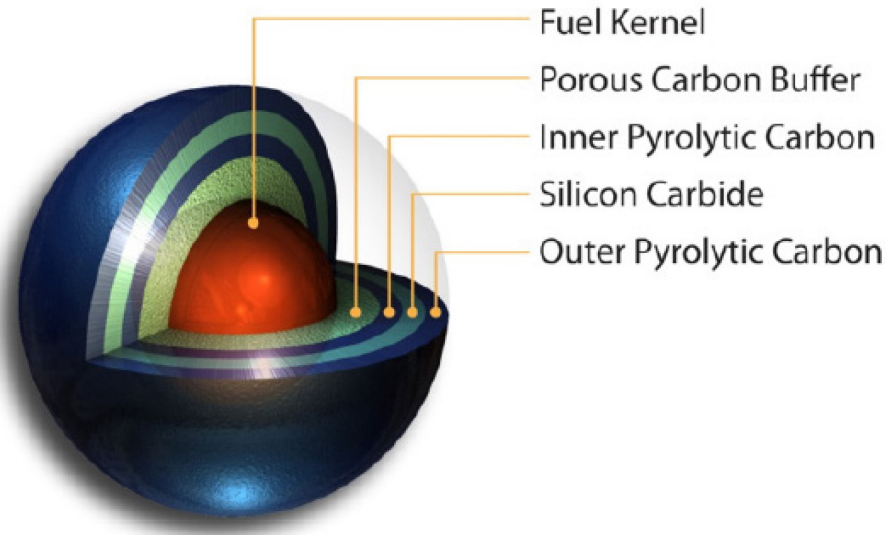


Figure 2. Typical TRISO-coated fuel particle geometry.

Table 1. Primary functions of particle fuel components.

Component	Primary Function
Kernel	Contains fissile fuel.
Buffer	Provides void space for fission product gases and accommodates differential changes in dimensions between coating layers and kernel.
IPyC	Structural layer and fission gas barrier that protects the kernel during SiC deposition and the SiC layer from most fission products during irradiation.
SiC	Primary structural layer and primary fission product barrier.
OPyC	Structural layer that also permits embedding the particles in graphitic matrix material.

The AGR-3/4 particles were made using LEU UCO kernels. The kernels were fabricated by BWX Technologies (BWXT 2006) in accordance with the AGR-3/4 DTF Fuel and Capsule Component Material Specifications (Marshall 2011). The UCO kernels were coated and characterized by Oak Ridge National Laboratory (Hunn 2007) (Kercher 2011). Coating was performed in accordance with the AGR-3/4 fuel product specification (Barnes 2006b) (Marshall 2011).

After coating, AGR-3/4 fuel was formed into cylindrical compacts. The compact matrix material was composed of graphite flake and a thermosetting resin. Prior to compacting, the fuel particles were overcoated with thick layers of compact matrix material. This overcoat was intended to prevent particle-to-particle contact and to help achieve the desired packing fraction of the fuel particles. Each AGR-3/4 compact contained driver fuel particles and 20 DTF particles (making up about 1% of all the particles in each AGR-3/4 compact) that were placed along its center axis (Figure 3). AGR-3/4 compacts were nominally 12.51 mm in length and 12.31 mm in diameter. A complete description of the fuel compacts, fission product monitoring system, physics analysis, and thermal analysis was presented in the final as-run report (Collin 2016).

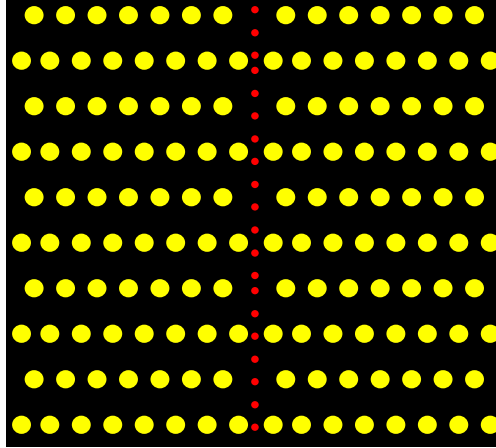


Figure 3. Schematic of an AGR-3/4 compact with DTF fuel particles (red) along the cylindrical axis of symmetry.

2.2. AGR-3/4 Description

To achieve the previously outlined test objectives in accordance with requirements from the technical program plan (Mitchell and Demkowicz 2022) and the irradiation test specification (Maki 2011), AGR-3/4 was irradiated in the northeast flux trap (NEFT) position of the ATR at INL. A cross-sectional view of the ATR core, which indicates the NEFT location, is displayed in Figure 4.

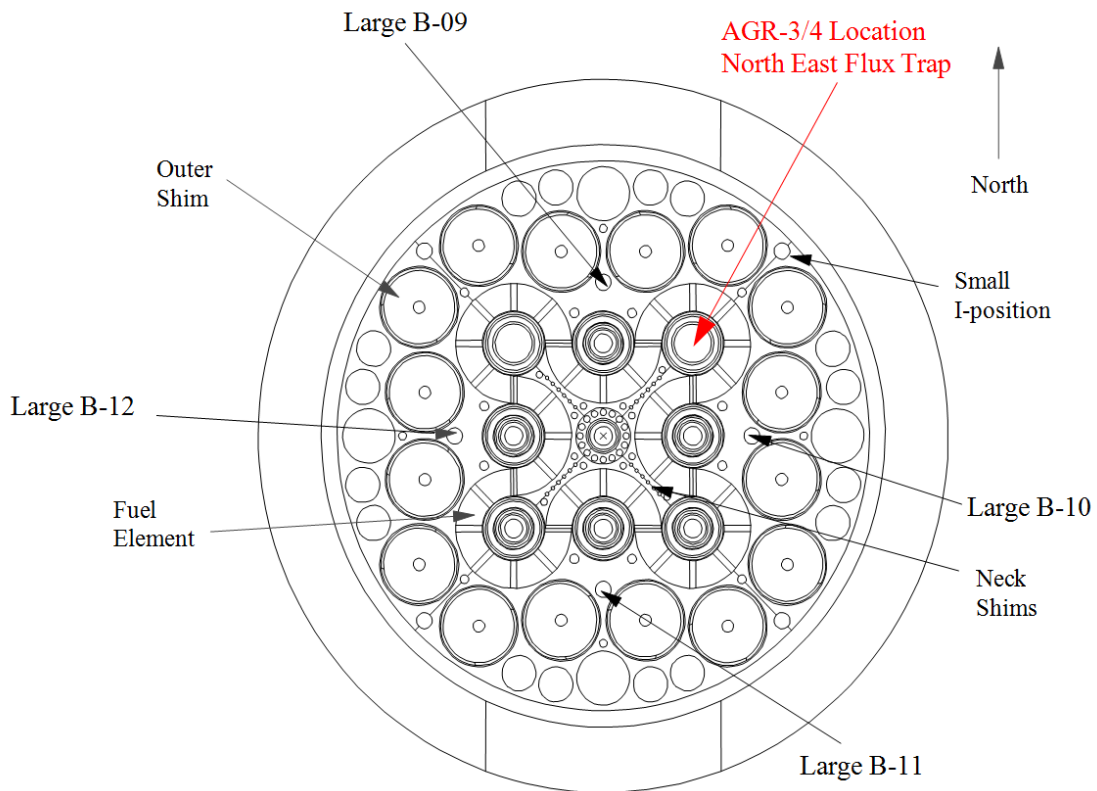


Figure 4. ATR core cross-section displaying the NEFT position.

The AGR-3/4 test train was a multi-capsule, instrumented experiment designed for irradiation in the 133.4-mm-diameter NEFT position of ATR. The best geometry for obtaining radial fission product transport data was determined to be a capsule with a single stack of fuel compacts that contained a known fraction of DTF particles surrounded by three concentric annular rings of test material: an annulus of fuel-compact matrix material (in some capsules graphite was substituted for this ring); an annulus of fuel-element graphite; and an annulus of graphite operating at a lower temperature to act as a sink for fission products. This configuration was intended to reduce axial temperature gradients and, therefore, axial diffusion. The test reactor's axial flux distribution and space considerations within the test train imposed a practical limit of 12 independently controlled and monitored capsules per test train. The capsules are stacked with Capsule 1 located at the bottom and Capsule 12 at the top. Similarly, the four compacts are stacked within each capsule with Compact 1 at the bottom and Compact 4 at the top. Hence, the compact naming convention begins with the capsule number followed by the compact number. For example, Compact 3-2 is located in Capsule 3 and is the second compact from the bottom. An axial view of the test train is illustrated in Figure 5. Figure 6 illustrates the radial view of a capsule.

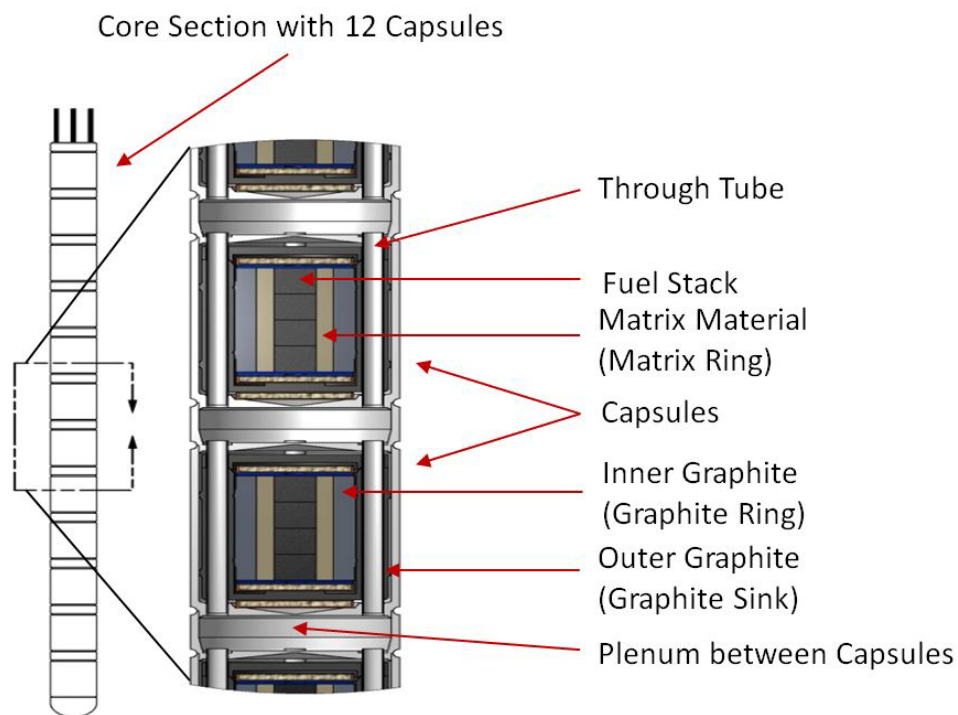


Figure 5. Axial schematic of the AGR-3/4 capsules.

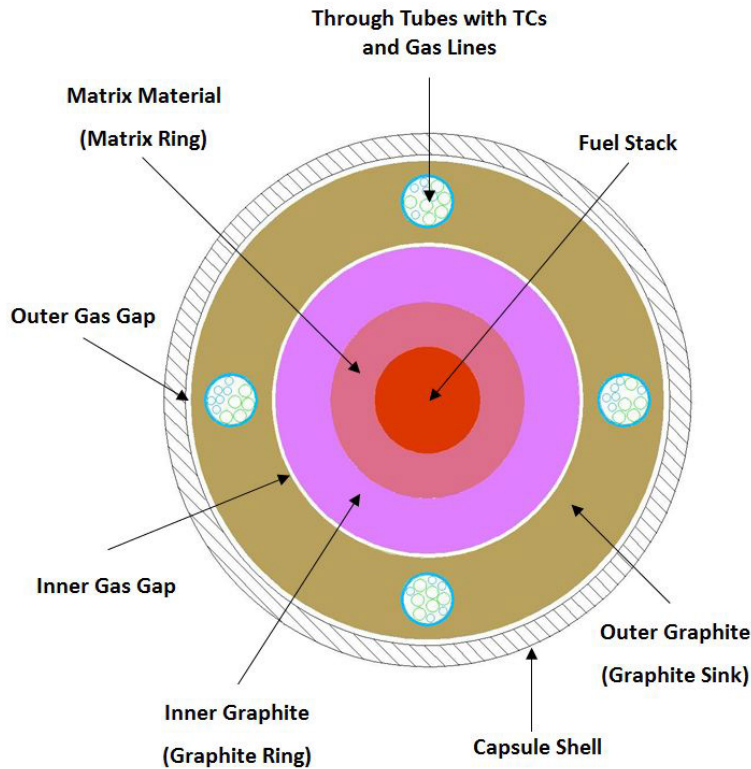


Figure 6. Radial schematic of the AGR-3/4 capsule.

2.3. AGR-3/4 Irradiation

AGR-3/4 combined the third and fourth irradiations in the AGR program. Irradiation began in December 2011 and concluded in April 2014 in the ATR for a total irradiation duration of 369.1 EFPD. Final burnup values on a per compact basis ranged from 5.35 to 15.24% fissions per initial heavy metal atom (FIMA), while fast fluence values ranged from 1.50 to $5.31 \times 10^{25} \text{ n/m}^2$ ($E_n > 0.18 \text{ MeV}$). Time-average volume-average (TAVA) fuel temperatures on a capsule basis at the end-of-irradiation (EOI) ranged from 854°C in Capsule 12 to 1345°C in Capsule 7.

After irradiation, the AGR-3/4 test train was transferred to the Materials and Fuels Complex HFEF at INL, and PIE activities were divided into two phases. The objectives of the AGR-3/4 PIE campaign are as follows (Demkowicz 2017):

- Determine the distribution of fission products in matrix and graphite rings at the (EOI).
- Determine the distribution of fission products in matrix and graphite rings at elevated temperatures following heating in pure helium and/or oxidizing atmospheres.
- Determine the fractional inventory of the fission products remaining in fuel kernels and the compact matrix at the EOI.
- Determine the fractional inventory of condensable and gaseous fission products released from fuel kernels and the compact matrix at elevated temperatures during heating in pure helium and/or oxidizing atmospheres.

2.4. Compact Re-irradiation

After over five years in storage, select compacts were re-irradiated in the NRAD reactor. The NRAD reactor is a 250 kW_{th} light water TRIGA (Training, Research, Isotopes, General Atomics) Mark II tank reactor (Bess, Briggs and Lell 2014) equipped with two beam tubes for neutron radiography. The NRAD core can be loaded with up to 64 fuel elements that are enriched to 19.75 wt% ²³⁵U mixed with zirconium hydride and erbium (UZrH-Er). These fuel elements are light water moderated and cooled using natural convection in the open tank. Moderator temperatures range between 26°C at startup to 37°C at-power operation. Graphite reflector assemblies surround the periphery of the reactor core to minimize neutron leakage. The number of fuel elements and graphite assemblies can be varied, along with their locations, to adjust core reactivity. A cross-section view of the core configuration of the NRAD reactor is provided in Figure 7 (Bess, Briggs, and Lell 2014). The select compacts were re-irradiated for approximately five days in the C4 irradiation position (see Figure 7), which according to bare foil gold foil measurements, experiences a neutron flux of 5.2×10^{12} n/cm²-s (Stempien et al. 2021).

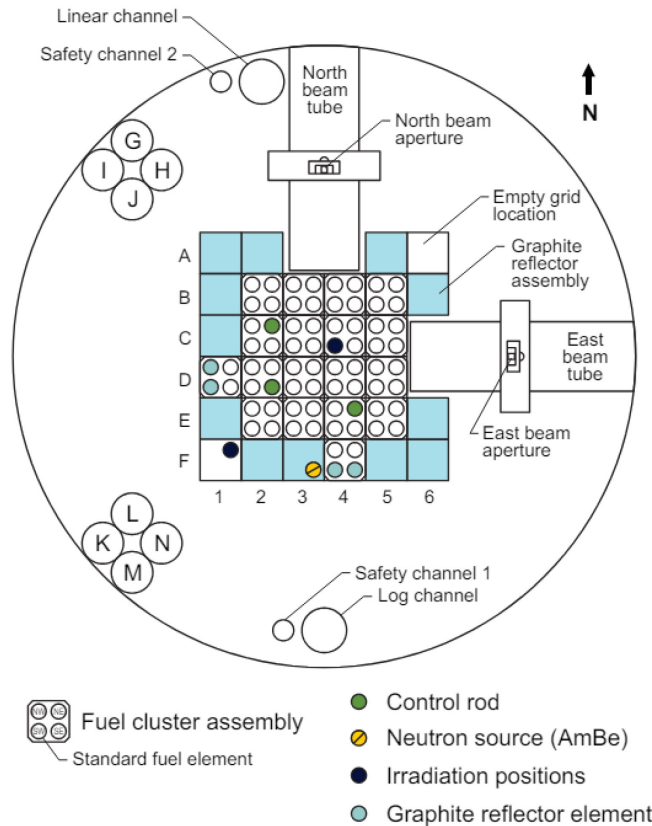


Figure 7. Cross section view of the NRAD TRIGA reactor core configuration.

2.5. Heating Tests

Comparisons between experimental heating test fission product measurements and model predictions focused on the short-lived fission products ¹³¹I and ¹³³Xe along with long-lived ⁸⁵Kr. The FACS furnace (Figure 8) at INL (Demkowicz et al. 2012) was used to heat the selected re-irradiated compacts separately at a predetermined target temperature. Helium sweep gas passed through the system at a flow rate of 1 L/min and the condensable fission products (e.g., ^{110m}Ag, ¹³⁴Cs, ¹³¹I) were collected on a condensation plate held on the end of a cold finger (Stempien et al. 2021). These plates were exchanged throughout the

tests and gamma counted upon removal from the furnace. The radionuclide inventories on each plate require correction by “collection efficiencies” for each condensable radionuclide to estimate the true inventory that was released from the fuel. The efficiencies are defined as the inventory of a given element collected on the plate divided by the total inventory released from the fuel. The collection efficiencies are intended to account for the inventory that was lost to other areas inside the furnace besides the condensation plates. In applying a single collection efficiency for each condensable radionuclide, the assumption is that the collection efficiency is constant throughout the test.

The FACS Fission Gas Monitoring System (FGMS) was used to collect and count ^{133}Xe and ^{85}Kr in charcoal-filled cryotraps over 4-hour intervals (Stempien et al. 2021). These collected measurements do not require a collection efficiency correction as calibration tests have confirmed that noble gas in the furnace chamber is completely transferred to the cryotraps during the tests. The long-lived fission product ^{85}Kr produced in the ATR irradiation was decay-corrected to the start of the FACS heating test. The accumulation of ^{85}Kr inventory from the NRAD re-irradiation is negligible when compared to the ATR irradiation (Stempien et al. 2021). The measured ^{85}Kr release from the FACS heating test was decay-corrected to the start of the FACS heating test and divided by the decay-corrected inventory (at the start of the FACS heating test) to determine the fractional release from the compact.

The collected activities from the short-lived fission products ^{131}I and ^{133}Xe were decay-corrected to the start of the FACS heating test. Further, the ^{131}I decay-corrected activities (to the start of the FACS heating tests) were divided by the predetermined FACS furnace condensation plate collection efficiencies summarized in Table 2 (Stempien et al. 2018; Demkowicz et al. 2012; Demkowicz et al. 2015). To determine the compact release fraction of the short-lived radionuclides (the ratio of measured inventory from the heating test to the total inventory produced in the compact during irradiation), the corrected measured activities were divided by the calculated predicted inventories produced during the NRAD irradiation decay-corrected to the start of the FACS heating test.

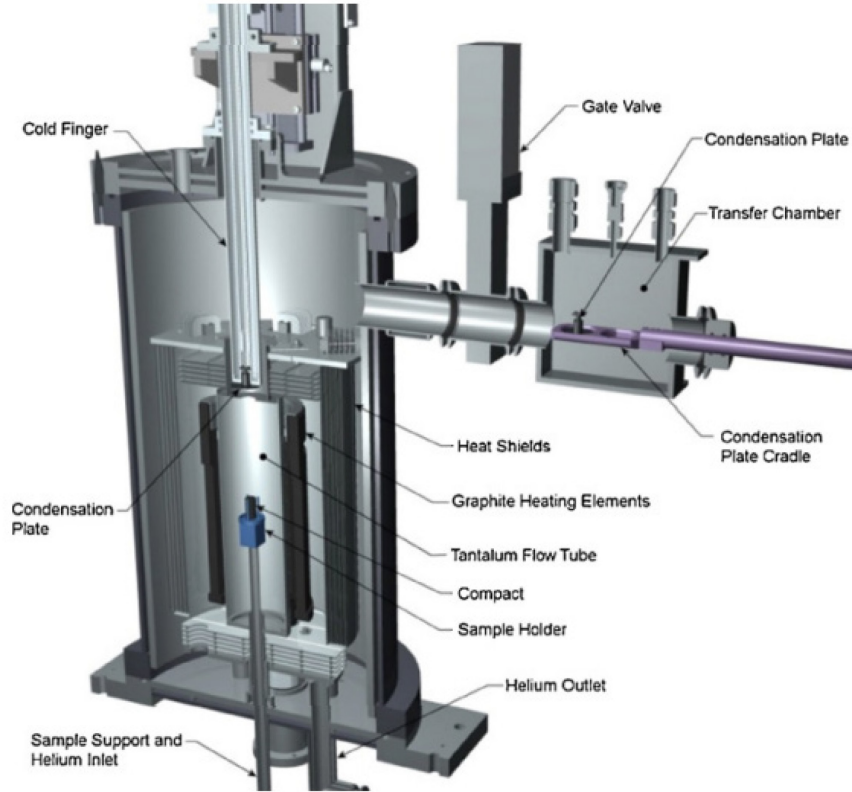


Figure 8. Graphic of the FACS furnace used to conduct heating tests.

Table 2. FACS furnace condensation plate collection efficiencies for ^{131}I .

Temperature	I-131
1000°C	0.100
1200°C	0.196
1400°C	0.348
1600°C	0.479

3. MODELING INPUT AND METHODOLOGY

BISON was used to model the evolution of the AGR-3/4 experiment from ATR irradiation to the FACS isothermal heating test to simulate the production, decay, and transport of select fission product species from both driver fuel and DTF fuel particles in a graphitic compact matrix. Key dates of interest to capture the compacts evolution are provided in Table 3 starting at the ATR EOI. Apart from the AGR-3/4 ATR EOI (Collin 2016), these dates were obtained from personal communications and have not been collectively summarized and published.

Table 3. Compact evolution from ATR irradiation to FACS heat testing.

AGR-3/4 ATR EOI	4/12/2014 5:00	
Compact 3-1	NRAD Re-irradiation Start Date	7/12/2019 8:38
	NRAD Re-irradiation End Date	7/17/2019 2:25
	FACS Start Date	7/25/2019 8:00
Compact 10-1	NRAD Re-irradiation Start Date	8/6/2019 8:01
	NRAD Re-irradiation End Date	8/11/2019 9:21
	FACS Start Date	8/16/2019 8:00
Compact 8-1	NRAD Re-irradiation Start Date	9/4/2019 9:10
	NRAD Re-irradiation End Date	9/9/2019 9:05
	FACS Start Date	9/17/2019 8:00
Compact 4-3	NRAD Re-irradiation Start Date	7/12/2021 8:58
	NRAD Re-irradiation End Date	7/17/2021 8:58
	FACS Start Date	7/23/2021 8:00

In addition, BISON assumes that the DTF particles fail at the beginning of the ATR irradiation, and there are no driver fuel particle failures during the irradiation and subsequent FACS heating tests (except for one compact, which is discussed below). Key aspects of the modeling of the AGR-3/4 irradiation and heating tests are described in the following subsections.

3.1. Input Parameters

The input parameters needed to model the AGR-3/4 experiment are provided in Table 4. They originate from these sources:

- The “AGR-3/4 Irradiation Test Final As-Run Report” (Collin 2016) for the fuel characteristics, particle geometry, compact characteristics, and material non-mechanical properties.
- A Combustion Engineering/General Atomics (CEGA) Corporation report for the material mechanical properties (CEGA 1993).

Fuel particle geometry and material attributes used in the BISON simulation are listed in Table 4. Where standard deviations are provided, the BISON simulation considers statistical variations for that

parameter. This includes kernel diameter, buffer thickness, IPyC thickness, SiC thickness, and OPyC thickness for the driver fuel particle and PyC thickness for the DTF particle.

Table 4. Parameters used to model the AGR-3/4 experiment.

Category	Parameter	Value
Fuel characteristics	U ²³⁵ enrichment (wt%)	19.717
	Oxygen/uranium (atomic ratio)	1.43
	Carbon/uranium (atomic ratio)	0.361
Particle geometry	Kernel diameter (μm)	357.3 ± 10.5
	Buffer thickness (μm)	109.7 ± 7.7
	IPyC thickness (μm)	40.4 ± 2.3
	SiC thickness (μm)	33.5 ± 1.1
	OPyC thickness (μm)	41.3 ± 2.1
	Particle asphericity @ SiC (aspect ratio)	1.056
Compact characteristics	Diameter (mm)	12.31
	Number of driver particles per compact	1872
	Number of DTF particles per compact	20
	Compact matrix density (g/cm ³)	1.603
	Uranium contamination fraction	3.5 × 10 ⁻⁵
Material properties	IPyC Weibull modulus	9.5
	SiC Weibull modulus	6
	OPyC Weibull modulus	9.5
	IPyC / SiC bond strength (MPa)	100
	PyC Poisson's ratio in creep	0.5
	PyC creep coefficient amplifier	2
	Kernel density (g/cm ³)	11.098
	Buffer density (g/cm ³)	1.10
	IPyC density (g/cm ³)	1.904
	OPyC density (g/cm ³)	1.900
	IPyC (post compact anneal) BAF	1.027
	OPyC (post compact anneal) BAF	1.021
DTF property	Pyrocarbon thickness (μm)	20.0 ± 0.9
	pyrocarbon density (g/cm ³)	1.988
	Anisotropy	1.243

3.2. AGR Irradiation Conditions

BISON evaluates fuel performance based on the compact power density determined by the associated burnup and fluence with a corresponding set of thermal conditions. For this analysis, compact-specific fluence and burnup results from neutronics analysis (Sterbentz 2015) and fuel temperature histories from thermal analysis (Hawkes 2016) that were performed to support the AGR-3/4 experiment campaign were used in the models. The fluence, burnup, and final TAVA temperatures for the selected compacts are provided in Table 5 (Collin 2016).

Table 5. Selected AGR-3/4 compacts EOI TAVA temperatures, accumulated fluence, and burnup.

Compact	3-1	10-1	8-1	4-3
ATR Burnup (% FIMA)	12.2	12.1	14.5	14.3
ATR Fluence (10^{25} n/m ²)	4.04	4.12	5.13	4.89
ATR TAVA Temperature (°C)	1138	1172	1165	1035
Heating Test Temperature (°C)	1600	1400	1200	1000

Each compact was modeled for the entire duration of the AGR-3/4 irradiation (369.1 EFPDs) with EOI values of burnup and fast neutron fluence summarized in Table 5. Burnup and fast neutron fluence were assumed to evolve accordingly to the time-resolved power density.

BISON has considerable flexibility relative to the application of thermal conditions affecting fuel particles. Previous BISON analyses used daily volume-averaged temperatures to simulate evolution at the compact- and particle scales. Due to the strong influence of temperature on fission product transport, analyses presented in this work used daily compact minimum temperatures (Hawkes 2016) to define compact surface temperatures. Elevated, spatially resolved temperatures within the compacts were sampled to define the surface temperatures of individual driver and DTF particles throughout the simulations. This refined approach eliminates a significant simplification in the compact/particle thermal histories, and its methodology is described in further detail in Section 3.5.3.

3.3. NRAD Irradiation Conditions

The re-irradiation of selected compacts was performed in the 250 kW TRIGA reactor NRAD. The re-irradiation duration for the four compacts is summarized in Table 6. It is assumed that the re-irradiation temperature was approximately 25°C, and all ¹³¹I and ¹³³Xe produced during the irradiation (minus that which is radioactively decayed) remained contained in the fuel kernel (ignoring fission product recoil) until the start of the FACS heating test (Stempien et al. 2021). The compact power history used to obtain the generation of fission products during the irradiation is described in detail in Section 3.5.

Table 6. Re-irradiation duration for select compacts in NRAD.

Compact	Duration (days)
3-1	4.74
4-3	5.00
8-1	5.00
10-1	5.06

3.4. FACS Heating Test Conditions

Apart from Compact 4-3, the heating test evolution for selected re-irradiated compacts are described in “Reirradiation and Heating Testing of AGR-3/4 TRISO Fuels” (Stempien et al. 2021). In general, the compacts were heated to approximately 300°C from ambient and held for approximately two hours before being heated to their target temperature. Although not formally documented at the time of this publication, the heating test evolution for Compact 4-3 was similar to Compact 10-1 as in both compacts were held at their respective targeted temperatures for approximately 307 hours. Compact 3-1 was heated to 1600°C and held there for only 210 hours. During the heating test for Compact 8-1 after approximately 90 hours at the target temperature, the condensation plate cold finger required repair, and the furnace was returned to ambient temperature for approximately 28 hours before being brought back to 1200°C for another 123 hours. A summary of the heating test evolution for each compact is illustrated in Figure 9.

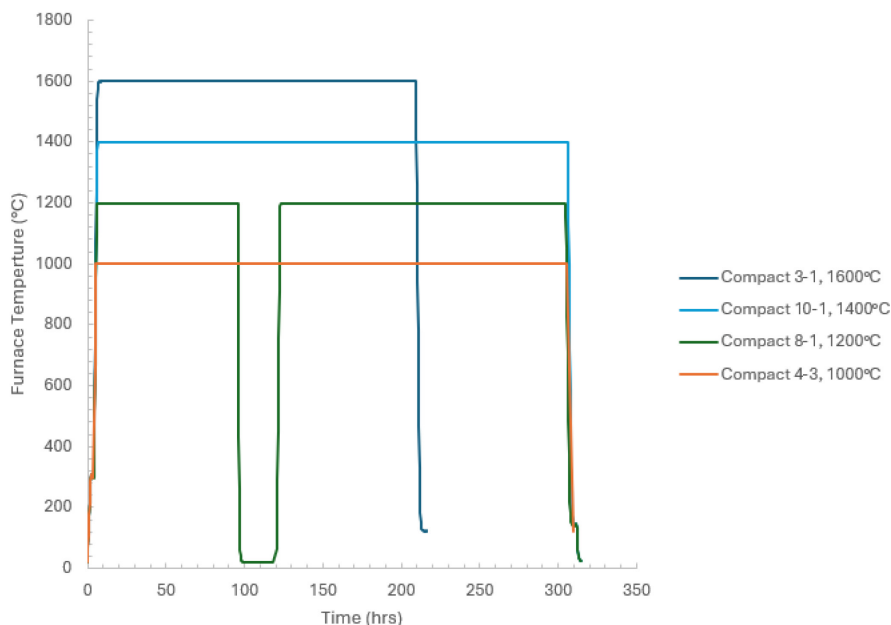


Figure 9. Evolution of the FACS furnace heating tests temperatures for selected re-irradiated AGR-3/4 compacts.

3.5. Fission Product Accounting

BISON currently includes source term models for elemental Ag, Cs, Sr, Kr, and Xe. For each element, the model calculates a production rate density $\dot{P} = f(\dot{F})$, where f is an element-specific function that may depend on fuel enrichment, burnup, and/or other factors. These source term models were primarily obtained from PARFUME. Unfortunately, their documentation is extremely limited, making it difficult to determine how they were developed and whether they are applicable to the broad range of experimental conditions being considered in this work. Furthermore, it is not clear whether the element-specific models are appropriate for modeling the specific nuclides of interest.

New nuclide-specific source terms were developed to address these limitations, assess the validity of the existing source term models, and eventually enable source term calculations for a much broader set of radionuclides. The source terms were developed using a workflow that uses Griffin, DRAGON5, and BISON. Griffin (Wang et al. 2024) is a MOOSE-based reactor physics application for multiphysics problems developed collaboratively by INL and Argonne National Laboratory (ANL). The Griffin team is currently verifying the cross-section preparation methodologies in Griffin, which rely on ENDF/B base data and the NJOY 2016 cross-section processing tool to generate custom fine group libraries for Griffin. The capability should be available in year 2025. In lieu of Griffin cross-sections, this report relies, in the interim period, on another tool to prepare nuclear data, DRAGON5 (Marleau et al. 2024). DRAGON5 is a lattice physics code developed at École Polytechnique de Montréal. DRAGON5 uses a collection of models to prepare microscopic neutron cross-sections for use in Griffin. DRAGON5 is limited to 297 isotopes for both cross-section data and decay and transmutation data based on ENDF/B-VIII.0. Griffin is deployed in the current work for depletion and transmutation analyses using these 297 isotopes but can be expanded in the future when native Griffin cross-section preparation is available.

The neutron cross-section process used in this work relies on obtaining the best possible estimate of the neutron energy spectrum in the sample of interest. DRAGON5 and other traditional lattice physics codes cannot model the ATR configuration, but the neutron spectrum obtained in DRAGON5 can be adjusted to match the spectrum of a higher resolution tool, for example, Monte Carlo N-Particle (MCNP).

Therefore, the amount of graphite holder in DRAGON5 was adjusted to match the historical spectrum from the original MCNP calculations (Sterbentz 2014). Figure 10 shows a comparison from the MCNP spectrum at different cycle times and the approximate spectrum obtained by adjusting the holder size. Note that this preliminary model does not include the Hafnium shroud. In the future, the Griffin model can be further improved to better simulate the capsule's environment. The DRAGON5 model was depleted at sample conditions of 195.65 W/g and a temperature of 1500.15 K. DRAGON5 treats the TRISO double heterogeneity effect and the spatial and energy self-shielding of neutrons. One energy group microscopic cross-section was tabulated as a function of burnup at 0., 0.098, 9.8, 19.6, 29.4, 39.1, 48.9, 58.7, 78.3, 97.8, 117.4, and 137.0 MWth/kgU.

Figure 10. Capsule 5 MCNP spectrum for various ATR fuel cycles versus approximated flux with a 3.0 cm graphite holder.

The Griffin model can be further improved in the future by achieving the following:

- Improve the spatial resolution of the capsule and surrounding regions
- Improve the neutron energy group resolution in the Griffin solution
- Deploy the Griffin on-line cross-section preparation with the double heterogeneity treatment to accurately represent the TRISOs within the compact and the methods for treating spatial and energy self-shielding effects in Griffin
- Compare results from ENDF/B-VII.1 and ENDF/B-VIII.0. ENDF/B-VII.1 includes 424 isotopes and ENDF/B-VIII.0 includes 557 isotopes with cross-sections data. Both libraries include 3,821 isotopes with decay and transmutation data.

3.5.1 Source term development

For the analysis of fission product release from re-irradiated compacts, the radionuclides of interest include ^{131}I , ^{133}Xe , and ^{85}Kr . BISON was applied to model the initial AGR-3/4 irradiation in ATR, compact re-irradiations in NRAD, and isothermal heating tests in FACS to aid in the interpretation of the fission products release measurements and other PIE results. For each nuclide of interest, BISON must model conservation of mass, which includes the effects of transport, production, and decay:

$$\frac{\partial c}{\partial t} = \nabla \cdot D \nabla c + \dot{F} \gamma - \lambda c,$$

where c is the molar nuclide concentration, t is the time, D is the effective Fickian diffusivity, \dot{F} is the fission rate density, γ is the nuclide fission yield, and λ is the nuclide decay constant. This work assumes that all nuclide transport at the particle and compact scales can be adequately described by concentration gradient-driven Fickian diffusion using the diffusivities given in (IAEA 1997).

While this work focuses on the analysis of fission product release from AGR-3/4, the multiphysics source term workflow was first applied to AGR-2 because its fuel structure and irradiation conditions are more similar to those that are expected to be used in commercial power reactor applications. AGR-2 experiment composition, geometry, and operating conditions (Collin 2018) were supplied to DRAGON5 to generate cross-section libraries for use in Griffin.

Griffin was then applied to model Compact 2-4-2 over the course of the AGR-2 irradiation. The simplified cross-sectional representation of AGR-2 used for the Griffin analyses, which includes a homogenized TRISO compact (center) and borated graphite holder (periphery), is shown in Figure 11.

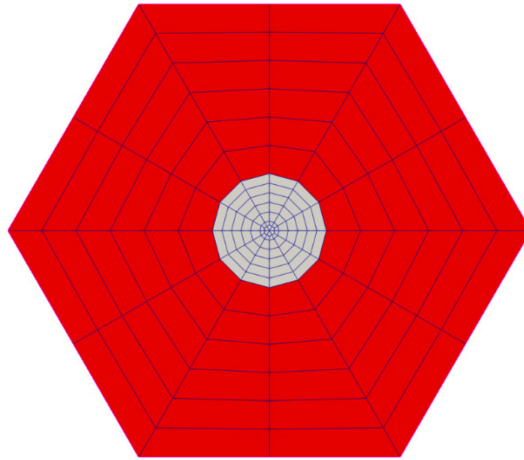


Figure 11. Simplified cross-sectional representation of AGR-2 used for Griffin depletion and transmutation analyses, which includes a homogenized TRISO compact (center) and borated graphite holder (periphery).

These analyses used AGR-2 power (Sterbentz 2014) and temperature conditions (Hawkes 2014) tabulated from Nuclear Data Management and Analysis System (NDMAS) (Hull, Plummer and Johnson 2020). For each depletion step, Griffin uses the current conditions and evaluated cross-sections to determine a representative neutron flux for use in depletion and transmutation calculations. Supplied and calculated linear powers, supplied average compact temperature, and calculated neutron flux from the Griffin calculations are shown in Figure 12. Precise agreement between the prescribed linear power (from NDMAS) and actual linear power (calculated from the Griffin-determined neutron flux) indicates that Griffin properly accounts for the time-varying influence of operating conditions and material evolution on the neutronic state of the system.

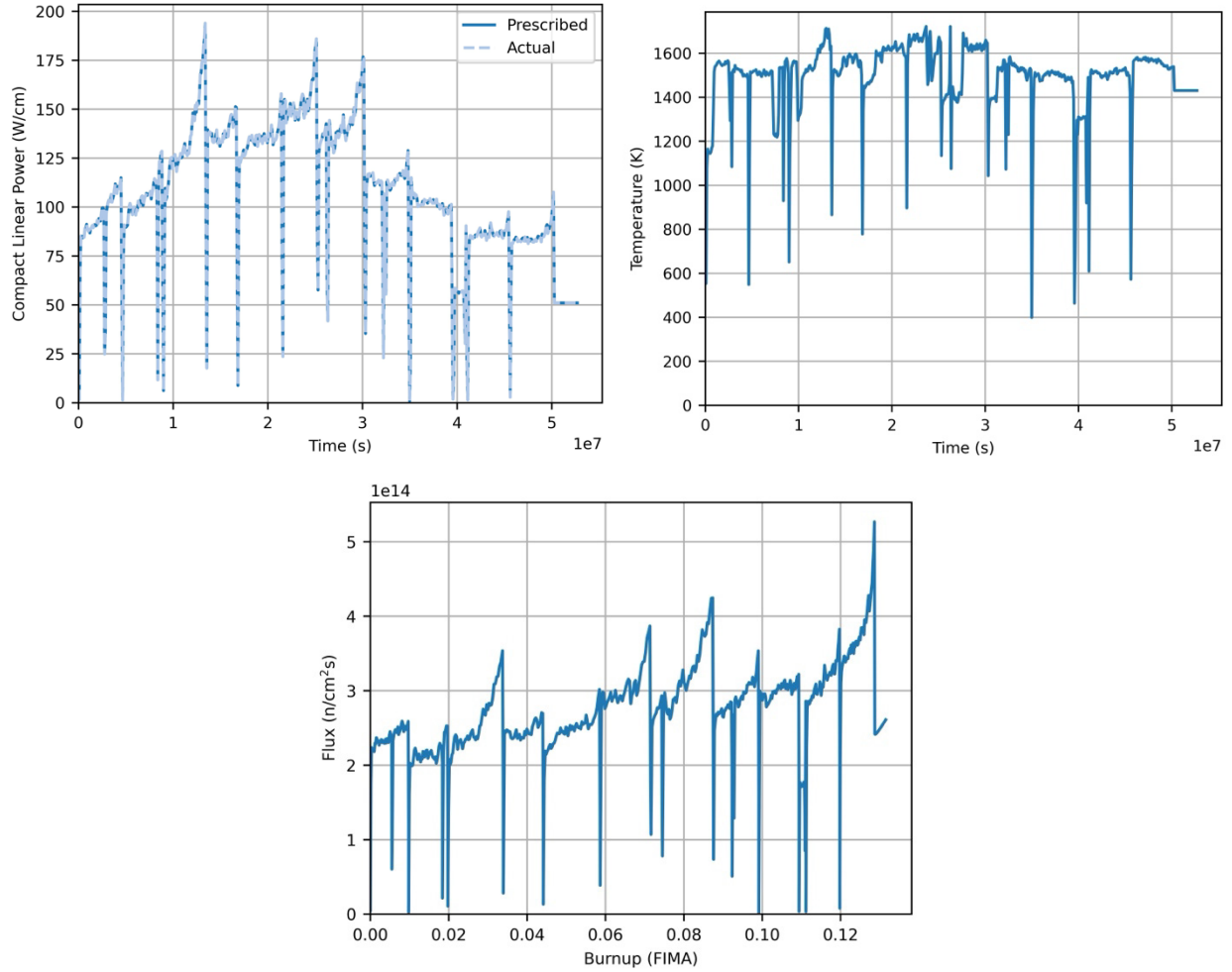


Figure 12. Examples of supplied and calculated linear powers (top left), supplied compact average temperature (top right), and calculated neutron flux (bottom center) from Griffin decay and transmutation simulations.

Predicted fuel compositions were compared to detailed AGR physics analyses performed using the MCNP and Oak Ridge Isotope Generation (ORIGEN) codes (when coupled to perform state and depletion calculations for AGR analyses, the two codes are collectively referred to as JMOCUP) (Sterbentz 2014), and cross-section dependencies were iteratively incorporated into the DRAGON model until the Griffin predictions adequately reproduced key behaviors from the existing MCNP/ORIGEN calculations. Ultimately, it was determined that fuel burnout and breeding, borated holder depletion, and temperature needed to be considered. The relative cumulative fissions (i.e., the ratios of total fissions by one nuclide to total fissions by all nuclides) of eight fuel nuclides predicted by Griffin are compared to EOI MCNP/ORIGEN predictions on log (left) and linear (right) scales in Figure 13. The results show ^{235}U accounts for almost all fission in the fresh fuel, as expected. As the irradiation continues, neutron capture, primarily by ^{238}U , and radioactive decay produce additional fissile and fissionable nuclides. Higher actinide concentrations are more sensitive to spectrum effects in the resonance regions, as shown in Figure 13, but this can be improved in future Griffin models.

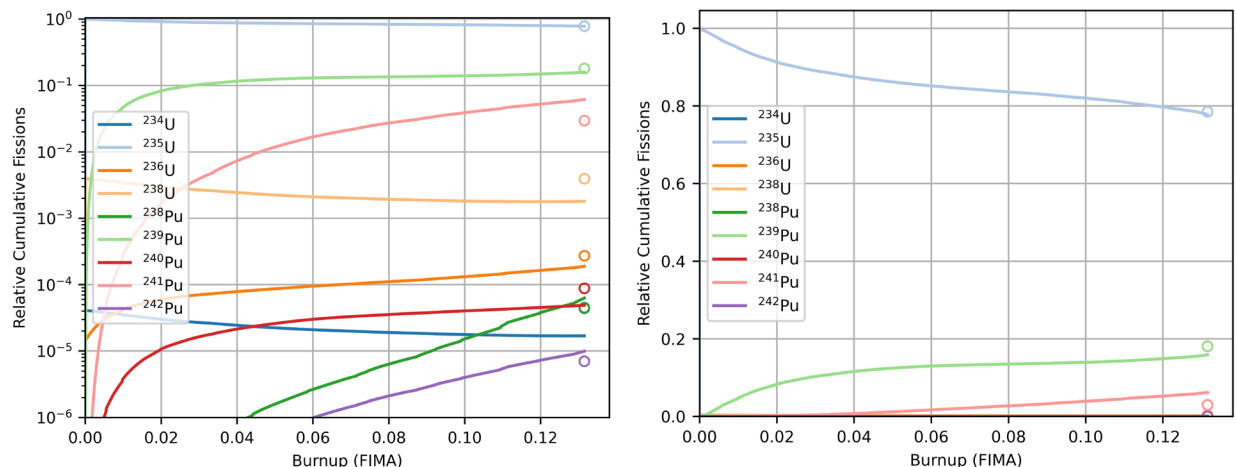


Figure 13. Relative fission yields of eight fuel nuclides predicted using the DRAGON–Griffin workflow (lines) compared to EOI MCNP/ORIGEN predictions from AGR-2 physics analyses (points). The same data are plotted on log (left) and linear (right) scales.

While differences between the Griffin and MCNP/ORIGEN predictions remain, particularly for nuclides with minor contributions to the total number of fissions, the results show that the DRAGON–Griffin workflow adequately captures the behavior of the three nuclides that produce the overwhelming majority of fission in AGR-2 fuel: ^{235}U , ^{239}Pu , and ^{241}Pu . Because each parent nuclide has different fission product yields, it is important to account for the effects of fuel composition evolution due to burnout and breeding to accurately predict fission product generation and subsequent transport and release. Favorable comparisons between the DRAGON–Griffin predictions and those of the high-fidelity MCNP/ORIGEN model lend credibility to the new approach, providing support for its use in developing new fission product source terms in the current work.

Additional time-resolved comparisons between the Griffin and MCNP/ORIGEN calculations are planned for future work to provide further support for the new approach. In the meantime, agreement between the EOI predictions is taken as sufficient justification to proceed with the new approach. For subsequent analyses in this work, the neutron spectrum of the AGR-3/4 experiment, its fuel composition, and its fuel geometry are assumed to be similar enough to that of AGR-2 to allow use of the AGR-2 depletion and transmutation calculations obtained from Griffin. Unfortunately, it is not clear how this assumption is likely to impact predictions obtained with the new nuclide-specific source terms, but the predictions are still expected to be more accurate than those that would be obtained using existing elemental source terms. Additional analyses focused on applying the new workflow to other AGR experiments and quantifying differences between them are planned for future work.

With confidence in Griffin and its predictions for this application, as demonstrated by the fuel nuclide comparisons shown above, it was then applied to model buildup and evolution of fission products. Griffin can predict the evolution of 1,690 fuel and fission product nuclides using an included decay-transmutation library (DTL). Predictions for the three nuclides of interest and other key isotopes associated with those elements are shown in Figure 14. EOI MCNP/ORIGEN predictions are included for comparison. Finally, elemental inventories, which are taken as the sums of all isotopes associated with each element, are also shown. Note that the elemental inventories include contributions from isotopes that do not appear in the plots. The xenon predictions are shown on a log scale to more clearly illustrate the ^{133}Xe results.

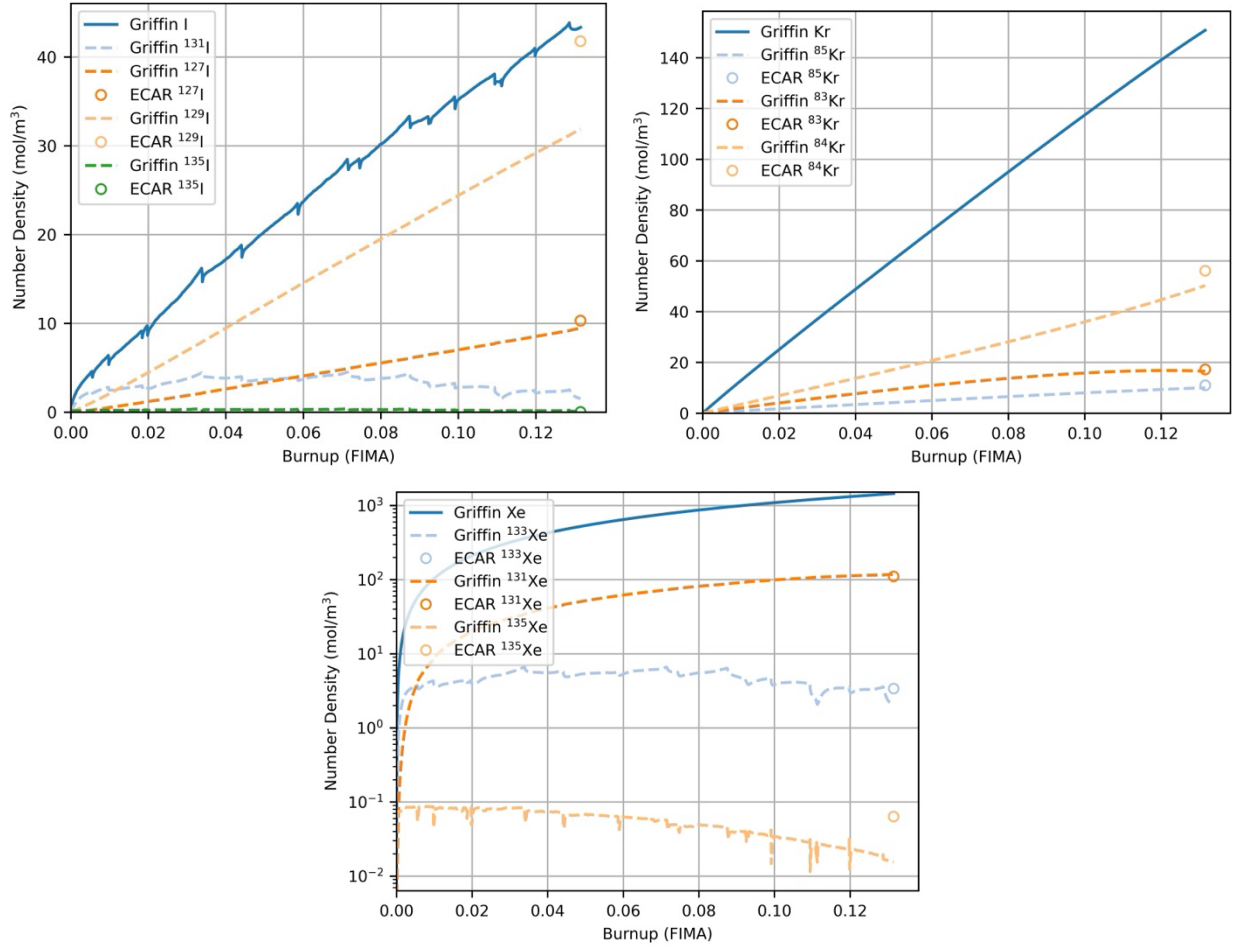


Figure 14. Evolution of the three nuclides of interest predicted by Griffin compared to EOI predictions from MCNP/ORIGEN. Other key isotopes associated with each element and elemental inventories are also included. Note that not all isotopes associated with each element are shown. The xenon predictions are shown on a log scale to more clearly illustrate the ^{133}Xe results.

Several features of these results warrant further discussion. First, data from nuclides with longer half-lives tend to be smoother and more linear, whereas data from nuclides with short half-lives tend to have jagged features. These jagged features, which arise due to radioactive decay during ATR shutdowns, can also appear in elemental results when a short-lived nuclide makes up a significant portion of the element's total inventory, as shown by the iodine results. The model adequately predicts the EOI inventory of ^{127}I and ^{135}I , but its ^{129}I predictions are less accurate. Unfortunately, no ^{131}I MCNP/ORIGEN results are available for comparison. Finally, the model appears to be very accurate for the other two nuclides of interest: ^{85}Kr and ^{133}Xe . These observations help to build additional confidence in the model and its predictions.

Griffin predictions for four additional elements (Ce, Cs, Eu, and Ru), for which AGR-2 PIE measurements are available (Hull, Plummer and Johnson 2020), are shown in Figure 15. The results show that the high-fidelity MCNP/ORIGEN predictions tend to agree very well with the PIE measurements. The more simplified Griffin results are less accurate but are generally representative of the expected results. These observations suggest that the Griffin model and/or the DRAGON cross-sections on which it is based, could be refined to improve their accuracy for this application. Nevertheless, its predictions are considered sufficiently accurate for the purposes of this work.

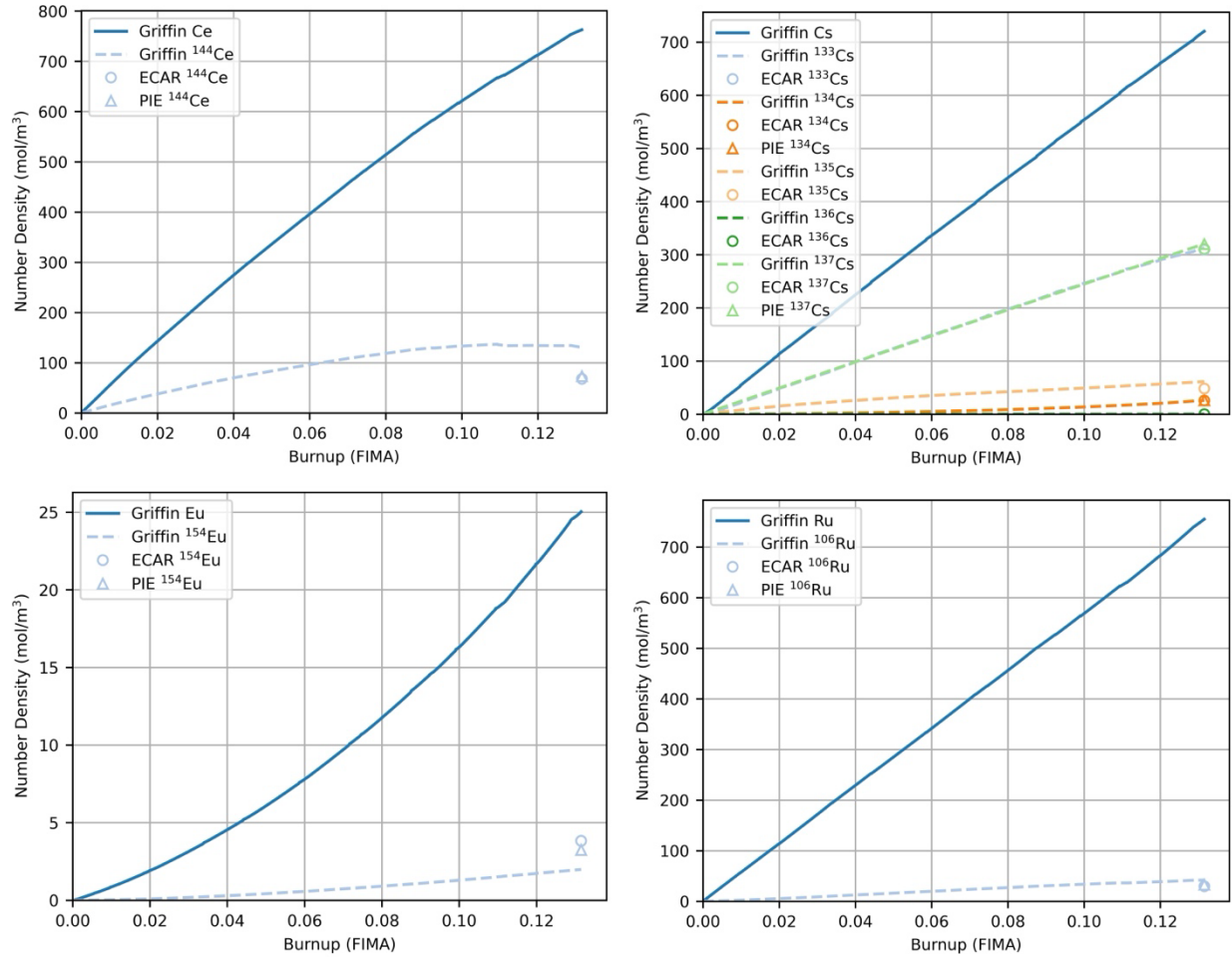


Figure 15. Evolution of the four additional elements and associated isotopes, for which MCNP/ORIGEN predictions and AGR-2 PIE measurements are available for comparison.

With improved confidence in the model's predictions, the Griffin calculations at each depletion step were used to derive more generally applicable source terms in the form of fission yield correlations. The assumptions, limitations, and details associated with this preliminary procedure are described in the following paragraphs. This approach relies on the observation that the AGR experiments conducted in ATR exposed TRISO fuels to similar temperatures and assumes that the effects of fuel burnout and breeding dominate fission product generation behaviors. Note that the implications of not correlating fission yields to temperature (and its influence on cross-sections) have not yet been fully explored. These effects will need to be assessed and quantified before this method of generating source terms for BISON can be endorsed for more widespread application. However, given the limited documentation available for the existing BISON source terms models (and noting that they also do not directly account for the effects of temperature), the new approach was considered acceptable for the current work.

Griffin accounts for decay and transmutation of all nuclides listed in its DTL. In many cases, nuclides have multiple production and loss terms, which include fission, neutron capture, and various forms of radioactive decay. This approach provides the most realistic description of composition evolution possible, but it is too complex for practical fuel performance analyses in BISON. In deriving simplified source terms for use in BISON, it was assumed that all nuclides are produced directly by fission. The validity of this assumption varies for each nuclide depending on the half-life(s) of its parent nuclide(s) and should be examined on a case-by-case basis.

Furthermore, it is assumed that all production and transmutation takes place in the kernel. Fission products are then free to transport anywhere within the particle or compact as determined by their chemical properties and decay at any time. This likely introduces some error, but it is not expected to be prohibitively high compared to other sources of error in these calculations and uncertainties associated with the existing source term models. It should be possible to perform analyses using full multiphysics coupling between Griffin and BISON. However, the computational expense associated with this approach is expected to be significantly higher, so it was considered beyond the scope of this work. Therefore, this report proceeds with an intermediate-level approach under the stated assumptions.

Under these assumptions, each nuclide has only one production term (e.g., fission). To isolate that production term for each nuclide of interest, a Griffin simulation was run under the additional assumption that the nuclide is stable. The results for select xenon isotopes are shown in Figure 16. The plot shows that omitting ^{133}Xe decay from the calculation dramatically increases ^{133}Xe , and therefore, also elemental xenon buildup in the fuel when compared to the results shown in Figure 14. This produces significant disagreement between the EOI Griffin and MCNP/ORIGEN predictions, as expected. Note ^{133}Xe inventory still tends to plateau due to its removal by neutron capture. The resulting nuclide number densities were used to fit the inventory-dependent fission yields that account for the effects of production and loss due to neutron capture. The details are discussed below. These discussions detail the procedure for ^{133}Xe . Analogous procedures were applied to ^{85}Kr and ^{131}I . Decay of the nuclides of interest is re-incorporated in BISON simulations as described later in this section.

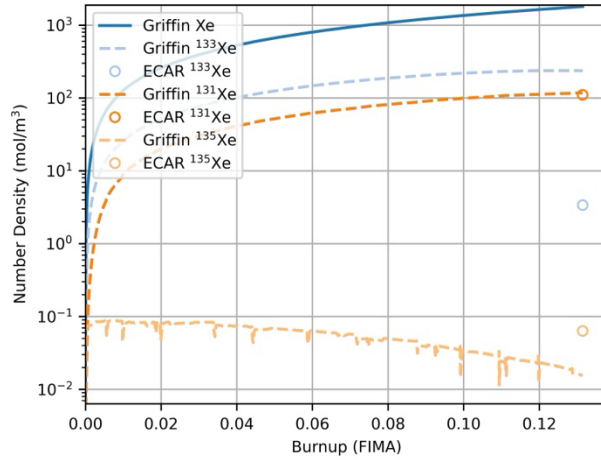


Figure 16. Evolution of selected xenon isotopes, including ^{133}Xe , which was assumed to be stable in this simulation to isolate its production for development into a nuclide-specific source term for BISON. Note that ^{133}Xe still tends to plateau due to neutron capture.

Griffin calculates nuclide number densities at each depletion step, which for these simulations, are evaluated at increments of one day or less over the course of the approximately 600-day AGR-2 irradiation. Currently, the heterogeneous structure of the TRISO fuel form, which consists of both particles (including UCO kernels) in a graphitic matrix, is represented as a single homogeneous domain. As such, the calculated number densities are average values over the entire compact. Compact and particle dimensions, therefore, were applied to scale the number densities such that the results were consistent with the assumption that all fission products are generated in the TRISO kernels.

For each depletion step n and corresponding time t_n , the number densities N_n were used to calculate an average production rate density \dot{P}_n :

$$\dot{P}_n = \frac{N_n - N_{n-1}}{t_n - t_{n-1}}.$$

The fission rate densities at each depletion step were then used to calculate average fission yields:

$$\gamma_n = \frac{2\dot{P}_n}{\dot{F}_n + \dot{F}_{n-1}}.$$

3.5.2 Fission product tracking

The average fission yields at each depletion step were correlated to the corresponding number densities using second order polynomials. This approach essentially incorporates loss of a nuclide due to neutron capture into its own fission production term. Production of a nuclide is reduced as its inventory increases toward a value where neutron capture becomes significant, yielding the plateau behaviors shown in the results above. This approach would clearly introduce error into downstream nuclide inventories, but this effect is mitigated by developing BISON correlations for each nuclide separately.

As a check, the inventory-correlated fission yields, inventories, and fission rates were used to recalculate nuclide number density evolution over the entire AGR-2 irradiation. The results are compared to the Griffin predictions from which they were derived, and results obtained using the existing BISON source term model in Figure 16. In this case, a linear scale was used to illustrate trends in both the ^{133}Xe and elemental xenon results more clearly. Recall that this simulation assumed that ^{133}Xe was stable, so the Griffin predictions and the corresponding fit are not expected to match the EOI MCNP/ORIGEN prediction, which includes the effects of decay and falls at about 3 mol/m^3 (see the log-scale results in Figure 15). The results show that the polynomial fit reproduces the data very well. Furthermore, close agreement between Griffin's elemental xenon predictions and those from the existing BISON source term model suggest that the model is intended to predict production of elemental xenon, rather than a particular isotope thereof.

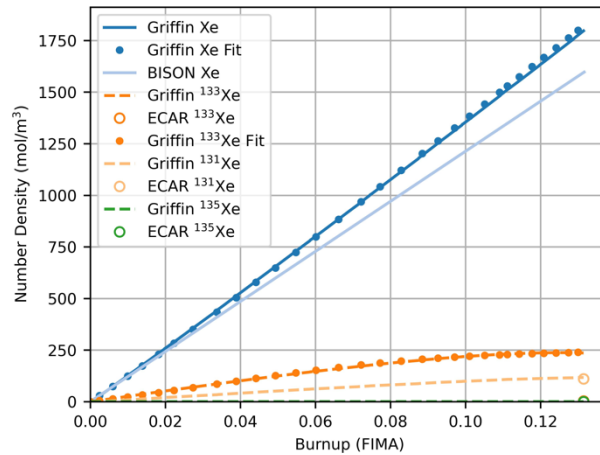


Figure 17. Evolution of selected xenon isotopes using Griffin, inventory-dependent fission yield correlations developed from Griffin results, and the existing BISON source term model. As before, ^{133}Xe was assumed to be stable to isolate its production term.

Similar comparisons are made for krypton and iodine in Figure 18. As was observed with ^{133}Xe , assuming that ^{131}I is stable drastically increases its inventory and that of elemental iodine when compared to the results shown in Figure 14. On the other hand, assuming that ^{85}Kr is stable has little effect on its inventory or that of elemental krypton. This makes sense because the half-life of ^{85}Kr (about 11 years) is long compared to the ATR irradiation time (about 600 days). As such, the ^{85}Kr inventory is not predicted to approach equilibrium. In contrast, ^{133}Xe and ^{131}I have half-lives of about 5 and 8 days, respectively. Their inventories are therefore predicted to reach equilibrium during the ATR irradiation when

accounting for radioactive decay. The combined results illustrate how ^{131}I and ^{133}Xe production are substantially higher than that of ^{85}Kr . This is consistent with the observation that the NRAD re-irradiation produced significant amounts of the short-lived nuclides but did not have an appreciable effect on ^{85}Kr inventory. As before, the results show that the polynomial fits reproduce the Griffin predictions very well, providing support for using them to define nuclide-specific source terms in BISON.

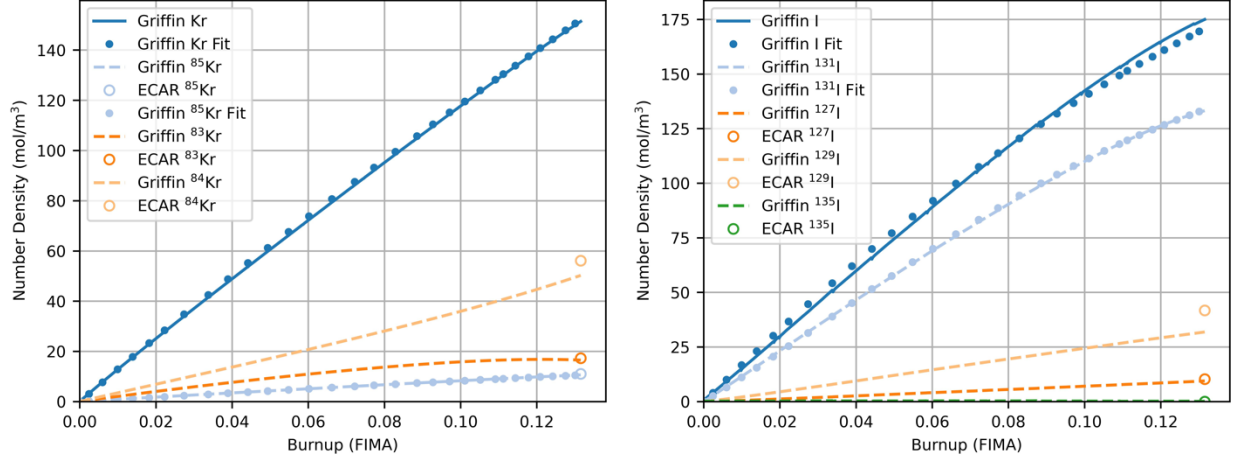


Figure 18. Evolution of selected krypton and iodine isotopes using Griffin and the inventory-dependent fission yield correlations developed from Griffin results.

The coefficients of the inventory-correlated fission yields are given in Table 7. At this early stage in source term model development, the correlations were implemented in BISON input files. Specifically, the correlations were supplied to MOOSE ParsedMaterial classes along with BISON-calculated inventories and fission rate densities to calculate temporally and spatially resolved nuclide production rate densities for use in particle-scale simulations. These and other new source term models will be considered for implementation in the BISON code in the future as work focused on their development, verification, and validation progresses. As mentioned above, the decay of each nuclide is accounted for in BISON using the mass conservation equation introduced at the beginning of this section, the BISON Decay class, and decay constants taken from the DTL used for the Griffin calculations.

Table 7. Coefficients of the nuclide-specific fission yields fit to inventories. The correlations have the form $\gamma = (aN_i^2 + bN_i + c)/1 \times 10^{30}$, where γ is the fission yield in mol/fission and N_i is the nuclide number density in mol/m³.

Nuclide	a	b	c
^{85}Kr	-5.367	-10.00	3432
^{131}I	-2.594	198.4	43420
^{133}Xe	-3.446	542.6	85460

As a final check, the new correlations and appropriate decay constants were used to model the evolution of the three nuclides of interest over the entire AGR-2 irradiation in BISON. The results are compared directly to the original Griffin calculations, which also included decay, in Figure 19. The results show that while BISON consistently underpredicts the inventories of all three nuclides, it generally captures their magnitudes and trends with a reasonable degree of accuracy. Specifically, BISON fairly accurately models the evolution of long-lived ^{85}Kr and short-lived ^{131}I . Its predictions for short-lived ^{133}Xe are less accurate but are still within a maximum relative error of about 20%. The sources of the non-constant errors between the BISON and Griffin predictions are still under investigation.

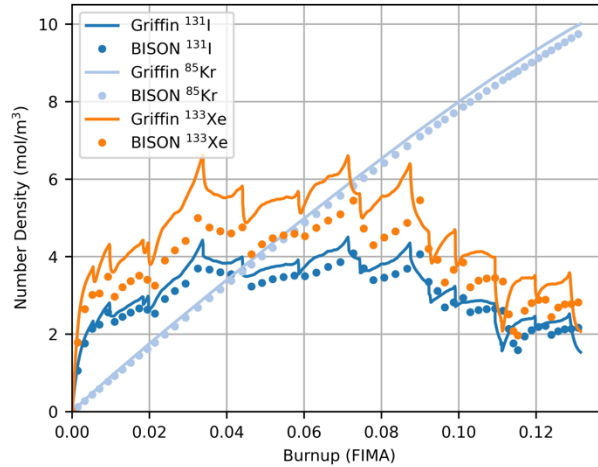


Figure 19. Final comparisons between Griffin and BISON predictions for the three nuclides of interest. The Griffin predictions include the effects of decay for all three nuclides. The BISON predictions were obtained using the new inventory-dependent fission yield correlations and also include the effects of decay.

It should be noted that BISON uses a simplified model to estimate fission rate density from a prescribed time-varying power density. The model uses a constant energy per fission, which ignores the substantial fuel composition evolution captured by the Griffin calculations. As a result, BISON and Griffin estimate that the AGR-2 compact accumulates approximately 13.2% burnup in about 574 and 610 days, respectively. Overall, and given the substantial simplifications associated with fission product generation, neutron capture, and decay employed in their development, the new source term models are considered very promising. The models were deemed acceptable for the purposes of this work, and the authors recommend their continued development as part of future work.

3.5.3 Multiscale BISON simulations

Multiscale BISON simulations were constructed to model the initial AGR-3/4 irradiation, re-irradiation, subsequent isothermal heating tests, and the periods of storage between them. MOOSE MultiApp functionality was leveraged to setup the multiscale simulations, with the compact scale as the main app and individual TRISO particles as sub apps. At the compact scale, the heterogeneous structure of the TRISO fuel form is represented as a single homogenized domain with effective material properties selected to represent the combined behaviors of particles imbedded in a graphitic matrix. The local power density and temperature within the compact are sampled to provide forcing functions and boundary conditions for particle simulations. At the particle scale, individual layers are resolved spatially, and heat and mass flux from particle surfaces are coupled back to the compact scale using point sources. Additional details about the compact- and particle- scale simulations are provided below.

Each AGR-3/4 compact is represented using a two-dimensional axisymmetric mesh. At a high level, BISON models transient heat conduction with generation and conservation of mass for the nuclides of interest. Time-resolved fast neutron fluences and minimum compact temperatures were taken from NDMAS and were used to calculate the compact thermal conductivity and to define the compact surface temperature boundary condition, respectively. Heat generation is modeled using spatially distributed point sources throughout the compact, each of which represent a single TRISO particle. The temperature calculation uses homogenized density, specific heat capacity, and thermal conductivity. The conservation of mass calculation uses diffusivities and decay constants. Key behavioral models, material properties, and the BISON classes used to model them are summarized in Table 8.

Table 8. Key behavioral models, material properties, and the BISON classes used to model them at the compact scale.

Behavior/Property	BISON Class(es)
Conservation of energy	HeatConductionTimeDerivative, HeatConduction, and TRISOMonteCarloPointSource
Conservation of mass	TimeDerivative, ArrheniusDiffusion, TRISOMonteCarloPointSource, and Decay
Density	Density
Thermal conductivity and specific heat capacity	GraphiteMatrixThermal
Diffusivity	ArrheniusDiffusionCoef

Monte Carlo methods are used to sample particle dimensions from truncated normal distributions based on the nominal AGR-3/4 particle designs and place the point sources associated with them within the compact. 20 DTF particle locations were placed randomly along the compact centerline, and 1872 driver fuel particle locations were placed randomly throughout the remainder of the compact such that no particles overlapped. Compact- and particle- scale simulations were iterated at every time step.

Each of the 1892 total particles in each compact is represented using a one-dimensional mesh that uses spherical symmetry, and the dimensions sampled above to define the kernel, buffer, IPyC, SiC, and OPyC layers. As with the compact scale, particle simulations model transient heat conduction with generation and conservation of mass for the nuclides of interest. Time-resolved power densities were taken from NDMAS and used to model power production in the kernel and calculate a fission rate density for use in the new fission product source term models. The particle surface temperature boundary condition was defined using spatially resolved temperatures from the compact scale as described above. Zero-value Dirichlet boundary conditions were applied to the particle surface to create sinks for diffusing nuclides. High, non-retentive diffusivities were applied to the IPyC, SiC, and OPyC of DTF particles to distinguish them from the driver fuel particles and capture the effects of their missing coating layers on fission product release. No mechanical deformation, buffer–IPyC gap formation, or explicit failure behavioral models were included in the analyses. Key behavioral models and material properties, as well as the BISON classes used to model them at the particle scale, are summarized in Table 9.

Table 9. Key behavioral models and material properties, as well as the BISON classes used to model them at the particle scale.

Behavior/Property	BISON Class(es)
Conservation of energy	HeatConductionTimeDerivative, HeatConduction, and FissionRateHeatSource
Conservation of mass	TimeDerivative, ArrheniusDiffusion, SpeciesSourceRate, and Decay
Density	Density
Thermal conductivity and specific heat capacity	UCOThermal, BufferThermal, HeatConductionMaterial, and MonolithicSiCThermal
Diffusivity	ArrheniusDiffusionCoef

The simulation setup described above allows for quantitative analysis of fission product generation, transport, and decay within the various DTF and driver fuel particle layers and the compact matrix. Release from particles, which is coupled to the compact scale production term can also be tracked on a per-particle basis. Finally, release from the compact itself can be quantified for comparison to PIE measurements. Successful comparisons require accurate irradiation and thermal histories for the re-irradiated AGR-3/4 compacts. Specifically, the analyses require a compact minimum (i.e., surface) temperature, fast neutron fluence, and power density throughout the initial AGR-3/4 irradiation, re-irradiation in NRAD, isothermal testing in FACS, and the two storage periods between them. The

procedure for constructing these histories for Compact 3-1 is detailed below. Similar procedures can be followed for other compacts.

3.5.4 Application to Compact 3-1

All the data necessary to simulate the initial AGR-3/4 irradiation were obtained from NDMAS, which tabulates the thermal (Hawkes 2016) and irradiation histories (Sterbentz 2015) of each compact over a period of about two years and four months. The data are tabulated in increments of EFPD, with the experiment lasting about 369.1 EFPD. BISON simulations were run under the assumption that the experiment was conducted at full power (i.e., 369.1 EFPD were accumulated over a period of 369.1 days). A 60-second shutdown to zero power and room temperature was appended to the initial AGR-3/4 irradiation history, which concluded on April 12, 2014, at 5:00 a.m. (Collin 2016). The fast neutron fluence was held constant for the remainder of the simulation due to a lack of NRAD data. The error associated with this simplification is expected to be small because the NRAD re-irradiation was much shorter and was expected to have a lower fast neutron flux than the initial irradiation in ATR.

Compact 3-1 was assumed to remain in storage at zero power and room temperature for about five years and three months until the NRAD re-irradiation began on July 12, 2019, at 8:38 a.m. (Table 3). As noted above, it was difficult to reconstruct the thermal and irradiation histories for the compacts while in NRAD. The BISON simulations held compacts at room temperature (25°C) throughout the re-irradiation under the assumption that the actual temperature was low enough to prevent appreciable fission product transport during that time. The compact power density while in NRAD is not known, so the time-averaged ratio of the power density to the fast neutron flux (6.544×10^{-11} J/m) was used to estimate a constant power density of 3.403×10^6 W/m³ from the nominal NRAD fast neutron flux of 5.200×10^{16} 1/m²-s. This comes out to approximately 4% of the time-averaged power density of the ATR irradiation. This approach relies on numerous assumptions about the experimental setups and neutron spectra associated with the two irradiations and is expected to be the largest single contributor to uncertainty in this work. Unfortunately, it is not clear currently how to construct more accurate NRAD histories or quantify the error introduced by this approach.

The BISON simulation for Compact 3-1 held the estimated power density constant for about five days until the re-irradiation ended on July 17, 2019, at 2:25 a.m. (Table 3). A 60-second shutdown to zero power was appended to the irradiation history as before. The power density was held constant at zero for the remainder of the simulation. Compact 3-1 was assumed to remain in storage at zero power and room temperature for about eight days until the FACS test started on July 25, 2019, at 8:00 a.m. (Table 3). Time-resolved compact temperatures are available for the FACS tests and were used directly in constructing the BISON simulations. The Compact 3-1 FACS test was conducted over a period of about nine days.

The Compact 3-1 BISON simulation was run with the preliminary NRAD power density described above. The predicted inventories of the three radionuclides at the end of the NRAD irradiation were too low when compared to the NRAD physics calculations, so the NRAD power density was iteratively increased to 5.615×10^6 W/m³ (an increase of about 65%) to yield relative errors of -2.93% and 6.27% for short-lived ¹³¹I and ¹³³Xe, respectively. As of this publication, the NRAD physics calculations have yet to be published, so the results presented herein should be considered preliminary. As was the case in the NRAD physics calculations, this analysis found that the inventory of long-lived ⁸⁵Kr at the end of NRAD was relatively insensitive to the NRAD power density. The resulting combined thermal and irradiation histories constructed to simulate Compact 3-1 in BISON are shown in Figure 20. Portions of the storage between the initial irradiation and NRAD re-irradiation are omitted to more clearly illustrate features of interest in the plots.

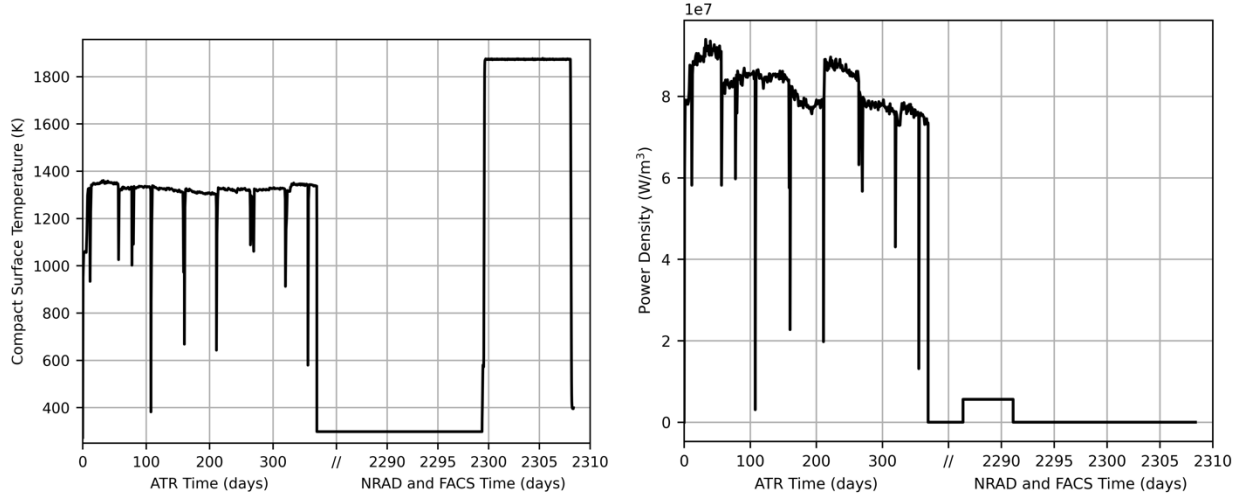


Figure 20. Combined thermal and irradiation histories constructed to simulate the initial AGR-3/4 irradiation, NRAD re-irradiation, and FACS testing for Compact 3-1 in BISON. Portions of the storage between the initial irradiation and NRAD re-irradiation are omitted to more clearly illustrate features of interest.

3.6 Fission Product Transport

Fission product transport in BISON is based on the fission product species (mass) conservation partial differential equation (Hales, et al. 2021b). Referring to the conservation of mass equation described in Section 3.5.1, BISON calculates the fission product diffusion based on the mass flux \mathbf{J} defined as:

$$\mathbf{J} = -D\nabla C$$

where the diffusivity D is calculated using the following Arrhenius-type equation:

$$D = D_{0,1}e^{-\frac{Q_{0,1}}{RT}} + D_{0,2}e^{-\frac{Q_{0,2}}{RT}}$$

where:

- $D_{0,i}$ = effective diffusion coefficient (m^2/s)
- $Q_{0,i}$ = activation energy (kJ/mol)
- R = gas constant (8.3142×10^{-3} kJ/mol/K)
- T = temperature (K)

The elemental based diffusivity pre-factors ($D_{0,i}$) and activation energies ($Q_{0,i}$) used in BISON for iodine, xenon, and krypton for the kernel and successive coating layers are derived from IAEA (IAEA 1997) and summarized in Table 10. The diffusion parameters in Table 10 were obtained by making the following assumptions:

- Diffusion for iodine, xenon, and krypton are similar and the same diffusivity pre-factor and activation energy can be used to derive the effective diffusivities for all three elements.
- Kernel data are based on UO_2 fuel due to the lack of experimental data and models for UCO fuel.
- The buffer and compact matrix provide no retention of the three fission products, and the effective diffusion coefficients are set to 10^{-8} m^2/s to allow for nearly instantaneous release from the buffer/compact.

- The effective diffusion coefficients derived can be applied to both normal operation and elevated isothermal heating conditions.

Table 10. Effective diffusivity pre-factors and activation energies used in BISON for iodine, xenon, and krypton.

Material	Temperature Range	$D_{0,1}$ (m^2/s)	$Q_{0,1}$ (kJ/mol)	$D_{0,2}$ (m^2/s)	$Q_{0,2}$ (kJ/mol)
Kernel	--	1.30E-12	126	--	--
Buffer	--	1.00E-08	--	--	--
IPyC/OPyC	--	2.90E-08	291	2.00E+05	923
SiC	< 1353°C	8.60E-10	326	--	--
	> 1353°C	3.70E+01	657	--	--
Compact matrix	--	1.00E-08	--	--	--

It is important to note the elemental diffusion parameters summarized in Table 10 have been derived from the evaluation of numerous irradiation and heating experiments to obtain effective diffusion coefficients for each layer. They are referred to as “effective” diffusion coefficients, “effective” meaning that all possible transport mechanisms are summarized in a single transport process. The use of these effective diffusion coefficients is to be considered with care. These coefficients were determined for UO_2 fuel and associated particle coatings of older German fabrication, whose properties (e.g., microstructure) are different than those of the UCO fuel and coatings of the AGR-3/4 experiment. Similar measurements for UCO fuel kernels (which can vary in stoichiometry) do not exist. Furthermore, in many cases, the coefficients employed here are partly based on data from post-irradiation heating tests and are conducted at higher temperatures than usual irradiation experiments. Consequently, IAEA diffusivities are not necessarily well adapted to model the fission product transport of the AGR-3/4 UCO fuel irradiation experiment.

The diffusivities of iodine, xenon, and krypton as a function of temperature in the successive layers of a particle are provided in Figure 21. The release of fission products is calculated at the compact level after the fission products were transported through both driver fuel and DTF particles and subsequently through the surrounding compact matrix. Fission products are considered released once they reach the compact edge. The fractional release of fission products is then calculated by normalizing the calculated release from the compact to the calculated kernel source or inventory.

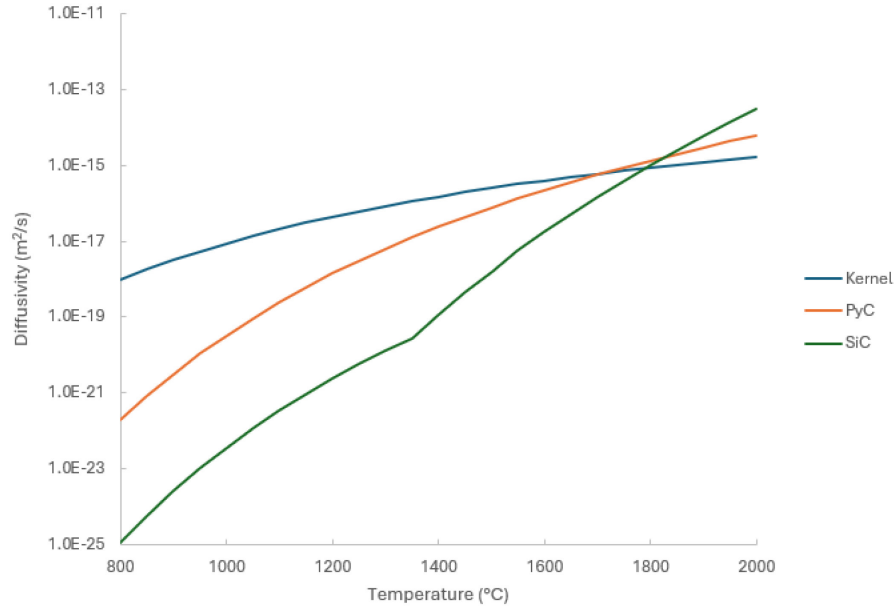


Figure 21. Diffusivities for iodine, xenon, and krypton as a function of temperature.

4. COMPARITIVE RELEASE RESULTS

Fission product release behavior during post-irradiation heating tests is complex and is dependent on fission product transport during ATR irradiation (^{85}Kr) and NRAD irradiation (^{131}I and ^{133}Xe). This includes the inventory that is released from DTF particles and driver fuel particles and the inventory of fission products held up in the OPyC layer at the end of irradiation. If the predicted distribution of retained fission products in the fuel at the end of irradiation differs substantially from the experiment, it could result in an appreciable difference between the predicted and measured heating test releases since the starting state of the fuel differs in the two cases. For example, condensable fission product release from a compact during a heating test may be dominated by inventory that was stored in the matrix at the end of irradiation (it is assumed that the radionuclides considered in this study will have no holdup in the compact matrix, so this phenomenon has negligible impact on the results). If the predicted release is dominated instead by the release from intact driver fuel particles, then the fact that the dominant releases arise from different phenomena should be considered when comparing the experiment to the model.

The predicted release fraction results are highly dependent on fission product diffusivities that are used to model the irradiations and heating tests. One objective of the AGR program is to generate diffusivities that are more reflective of the current TRISO fuel. Updating the diffusivities for the kernel, particle layers, and compact matrix will result in a more accurate prediction from these models during irradiation. The more accurately these codes can predict the fission product inventory end state after irradiation, the less uncertainty there will be from the heat testing results. Ideally, the fission product inventory at the end of irradiation in the driver fuel particles, DTF particles and in the compact matrix would be experimentally quantified and available as an input into the model to more accurately predict the release during the heating tests.

For this analysis, it is assumed that all DTF particles fail at the onset of the ATR irradiation in the fuel performance model. Based on a previous analysis of the AGR-3/4 irradiation and subsequent heating tests (Skerjanc 2023), it is also assumed that driver fuel particles remain intact during both irradiations and subsequent heating tests (with the exception of Compact 10-1, which will be discussed in Section 4.2).

Fractional release (M/C) is calculated by dividing the release (M) by the calculated inventory (C). From (Stempien et al. 2021), the experimental release measurements (M_E) were decay-corrected to the

start of the FACS heating tests and as-run physics calculations (C_E) were used to predict the inventory at the beginning of the FACS heating test. To be consistent with the measured results, the predicted release calculated by BISON during the heating test (M_B) was also decay-corrected to the start of the FACS heating test and the inventory of the radionuclides produced predicted by BISON (C_B) during irradiation (^{131}I and ^{133}Xe from NRAD and ^{85}Kr from ATR) was decay-corrected to the start of the FACS heating test to obtain the BISON predicted fractional release (M_B/C_B).

With all of this taken into consideration, the predicted fission product release fractions as calculated by BISON were compared to experimental results for all four compacts. These results are summarized in Figure 22 with the total release reported in particle equivalents at the end of their respective heating tests. To be consistent with (Stempien et al. 2021), the BISON results below assume 1,898 driver fuel particles and 20 DTF particles for a total of 1,918 particles resulting in one particle equivalent equal to a compact fraction of 5.21×10^{-4} . The final AGR-3/4 irradiation as-run report (Collin 2016) specifies 1,872 driver fuel particles and 20 DTF particles. Initial experimental results from Compacts 3-1, 8-1, and 10-1 were published in (Stempien et al. 2021). Since this publication, the FACS furnace collection efficiency and physics calculations have been refined, resulting in the experimental release values presented herein differing slightly. The experimental results have yet to be formally published for Compact 4-3 so the results presented herein should be considered preliminary.

The remainder of this section compares the experimental measured release to the BISON predicted release at both compact and radionuclide level. The following notes and generalizations on the results are made and are applicable to the four compacts:

- The time-dependent release is presented in linear and log scale to allow for visual inspection between compacts that experienced different orders of magnitude of fission product release.
- The measured uncertainties for ^{85}Kr and ^{133}Xe were about 10% and 15%, respectively (Stempien et al. 2021).
- The measured uncertainty for the condensable fission product measurements (^{131}I) was approximately 6% (Stempien et al. 2021).
- NRAD AGR-3/4 compact specific re-irradiation physics calculations to obtain the estimated compact fission product inventory (C_E) and subsequently used to calculate the measured fractional release (M_E/C_E) have not been formally documented.
- The BISON predicted release results decrease as the FACS target heating test temperature decreases (see Figure 22). This result verified that the BISON simulation is at the very least correctly capturing the physics of simulating fission product transport of the three radionuclides analyzed in this study.
- The intention of this report is to compare the measured to predicted fission product release results and not to analyze or hypothesize experimental measured release phenomena. Where it is appropriate to provide context to the discrepancies between the measured and predicted values, this report provides such insight, but the reader is encouraged to seek additional publications that provide greater context (Stempien et al. 2021; Stempien et al. 2018; Collin 2016).

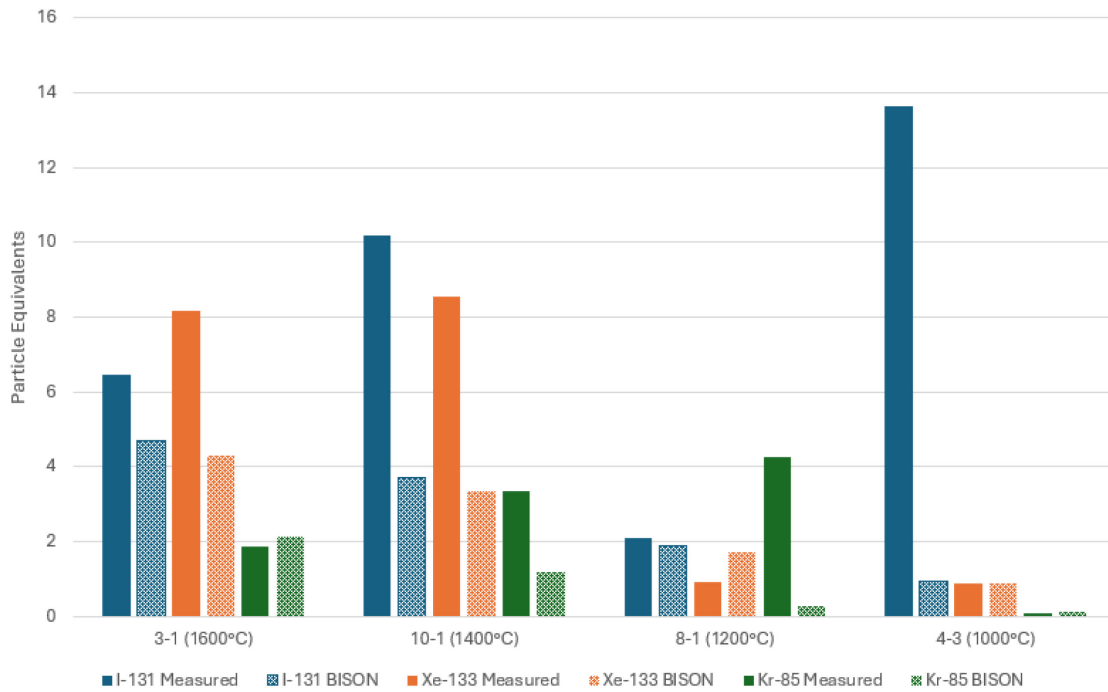


Figure 22. Summary of total particle equivalent release at the end of FACS heating tests. Note that the compacts are presented from left to right in decreasing FACS heating test temperature. Results from Compact 10-1 include a failed driver fuel particle 18 hours into FACS testing.

4.1 FACS Heating Test of Compact 3-1 at 1600°C

The time-dependent measured and BISON predicted release during the 1600°C FACS isothermal heating test of Compact 3-1 is summarized in Figure 23. The FACS furnace was held at temperature for approximately 202 hours, and the resulting release at the end of the heating test is summarized in Table 11.

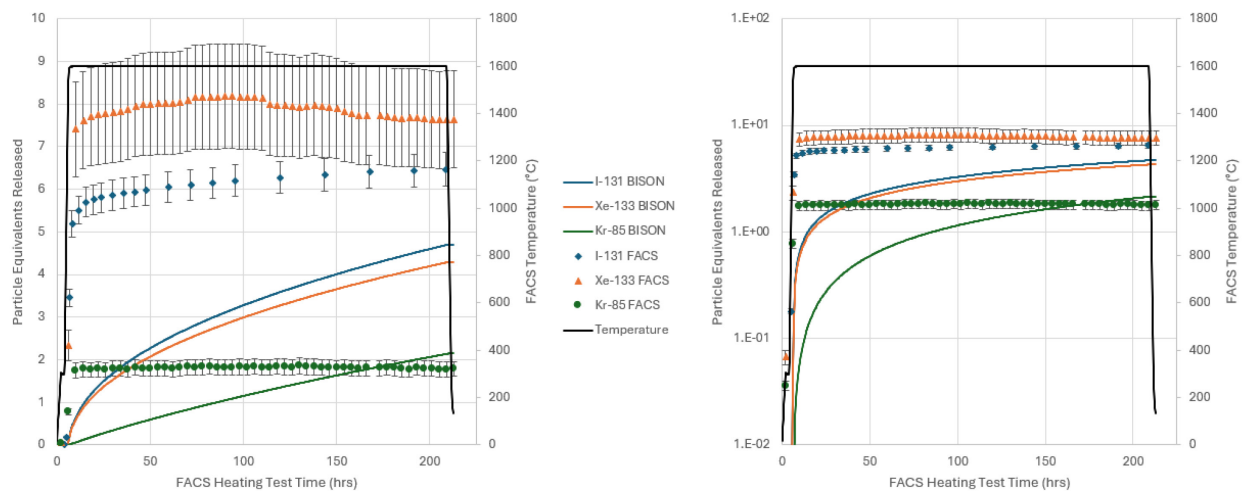


Figure 23. Time-dependent measured release from Compact 3-1 at 1600°C. The same data are plotted on linear (left) and log (right) scales.

Table 11. Total release from Compact 3-1 at 1600°C.

Nuclide	Particle Equivalents		Relative Error
	Measured	BISON	
I-131	6.47	4.70	-27%
Xe-133	8.18	4.29	-48%
Kr-85	1.85	2.14	16%

Referring to Figure 23, measured release results from Compact 3-1 warrant further discussion. In Figure 23, the cumulative measured release of ^{133}Xe and ^{85}Kr reach peak values and then decrease as the heating test progresses. In reality, this phenomenon is physically impossible since the release is cumulative. It is postulated that this is a result of the relocation of these two isotopes during counting within the bulk of the charcoal in the cryotrap, moving it farther from the detectors (Stempien et al. 2021). As such, the values reported in Table 11 represent the maximum measured values during the FACS heating test.

In general, BISON underpredicts the release of the short-lived fission products ^{131}I and ^{133}Xe by 27% and 48%, respectively. Since the release fraction is a ratio of predicted release to predicted inventory (M_B/C_B), making the release fraction independent from concentration would infer that BISON is underpredicting the total release of ^{131}I and ^{133}Xe by 27% and 48%, respectively. For example, if the calculated inventory is increased by 25%, the resulting total release would also increase by 25%, resulting in the same M_B/C_B release fraction. Therefore, when compared to the measured values, the differences between the BISON fission product transport results can be attributed to several factors that influence fission product transport, including kernel and layer diffusivities, spatial distribution of temperature, retention of fission products in the compact matrix, and possible release of the short-lived fission products during NRAD irradiation and prior to FACS heating tests.

4.2 FACS Heating Test of Compact 10-1 at 1400°C

It is speculated that Compact 10-1 experienced a failed driver fuel particle at approximately 18 hours into the FACS heating test (Stempien et al. 2021). Therefore, to be consistent with the measured results, the BISON simulation was evaluated to include a failed driver fuel particle at approximately 18 hours. Since it is assumed that the predicted release is from the 20 DTF particles, the release calculated by BISON is increased by 5%, the contribution from one DTF particle, to simulate a driver fuel particle failure at 18 hours. This methodology is a crude estimate to predict the release from a failed driver fuel particle and is more applicable to the contribution from short-lived fission products. For ^{85}Kr , where the inventory is generated from the ATR irradiation and held up in the TRISO particle, this methodology needs to be revisited in future applications where a more rigorous analysis of fission product tracking is required to account for rapid release from a failed driver fuel particle. Using this methodology, the time-dependent measured and BISON predicted release during the 1400°C FACS isothermal heating test of Compact 10-1 is summarized in Figure 24. The FACS furnace was held at temperature for approximately 300 hours, and the resulting release at the end of the heating test is summarized in Table 12.

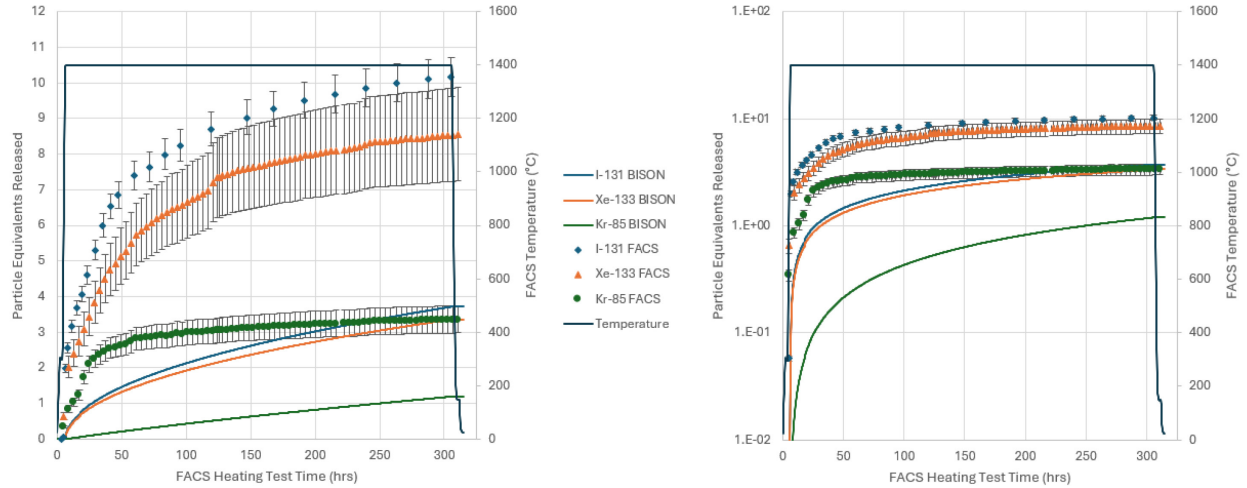


Figure 24. Time-dependent measured release from Compact 10-1 at 1400°C. The same data are plotted on linear (left) and log (right) scales.

Table 12. Total release from Compact 10-1 at 1400°C.

Nuclide	Particle Equivalents		Relative Error
	Measured	BISON	
I-131	10.16	3.72	-63%
Xe-133	8.54	3.36	-61%
Kr-85	3.36	1.20	-64%

For all three isotopes, BISON underpredicts the total release by approximately 60%, even when including a failed driver fuel particle early during FACS heating test in the BISON simulation. When compared to Compact 3-1, the ^{131}I and ^{85}Kr total measured release from Compact 10-1 was higher at the end of the FACS heating test even though the isothermal heating temperature was 200°C lower. Some of these differences can be attributed to the failed driver fuel particle early in the irradiation that is not modeled in BISON explicitly. This can also be due to overpredicting the inventory in the particles by the physics calculations (C_E) and/or underpredicting the fission products released from the particles (M_B). From the experiment perspective, it is unclear why the measured ^{131}I release from Compact 10-1 is higher than Compact 3-1 since both compacts had similar burnups and nearly the same TAVA temperatures (Stempien et al. 2021). For ^{85}Kr , if the fission product accounting is not properly represented in BISON (production or retention in driver fuel particles), the sudden release from the failed driver fuel particle during the heating test can be substantially mischaracterized. As far as the short-lived isotopes, it is encouraging to see the temperature-dependent BISON release profiles following similar trajectories to the measured profiles, albeit with different magnitudes.

4.3 FACS Heating Test of Compact 8-1 at 1200°C

The time-dependent measured and BISON predicted release during the 1200°C FACS isothermal heating test of Compact 8-1 is summarized in Figure 25. The FACS furnace was held at temperature for approximately 272 hours, and the resulting release at the end of the FACS heating test is summarized in Table 13.

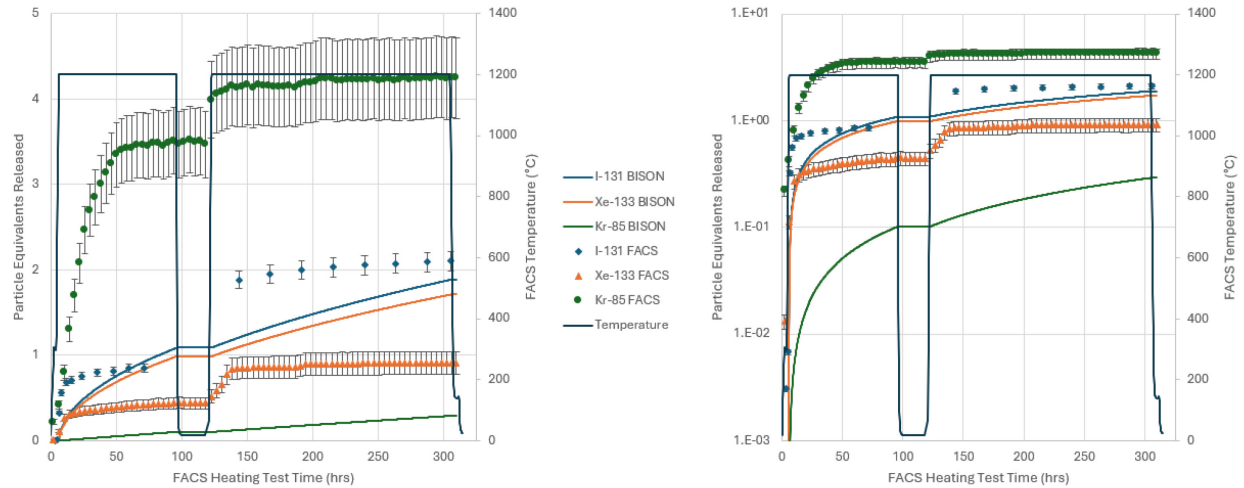


Figure 25. Time-dependent measured release from Compact 8-1 at 1200°C. The same data are plotted on linear (left) and log (right) scales.

Table 13. Total release from Compact 8-1 at 1200°C.

Nuclide	Particle Equivalents		Relative Error
	Measured	BISON	
I-131	2.10	1.88	-10%
Xe-133	0.91	1.71	88%
Kr-85	4.24	0.29	-93%

During the FACS heating test of Compact 8-1, the target FACS temperature of 1200°C was held for approximately 90 hours before being cooled back to ambient temperature due to an issue with the condensation plate cold finger (Stempien et al. 2021). Once the cold finger was repaired, the FACS temperature was brought back up to 1200°C at 120 hours, reaching the target temperature at 123 hours, and was maintained for 182 hours. This resulted in Compact 8-1 being exposed to an isothermal heating test temperature of 1200°C for a total of 272 hours. The observed step-change in measured fission product release post-cold finger repair is not addressed in (Stempien et al. 2021) but the paper does confirm that there was no indication of any driver fuel particle failures during the temperature evolution. This fission product release time-dependent evolution is not reflected in the BISON calculations, remaining unchanged during the cold-finger repair with a continuous increase as the FACS furnace is brought back up and maintained at the target temperature.

The predicted ^{131}I release by BISON at the end of the FACS heating test was in fairly good agreement with the measured value, underpredicting the total release by only 10%. The same is not true for ^{133}Xe , which was overpredicted by almost 90%. Conversely, BISON underpredicts the total ^{85}Kr by more than 90%. Compared to Compact 3-1, which was heat tested at 1600°C, the measured ^{85}Kr release from Compact 8-1 at 1200°C is almost 2.3 times higher even though the isothermal heating test temperature was 400°C lower. It is speculated that this difference is due to the release of the majority of the ^{85}Kr inventory from the DTF particles in Compact 3-1 during the ATR irradiation (Stempien et al. 2021), which depleted the available inventory of ^{85}Kr that could have been available for release. As will be discussed later in Section 4.7, this is not captured in the BISON simulations due to spatial temperature distribution discrepancies in the compact and/or the assumptions made for the radionuclide kernel and layer diffusivities. In addition, the measured and predicted release curves differ considerably throughout the heating tests. The measured release data increases rapidly for all three isotopes followed by a

substantial decrease in release rates such that the curves remain flat. The BISON model predicts gradual increase in release at the start of the heating test while maintaining a relatively constant release rate during the latter part of the test suggesting that the simulation is predicting different release phenomenon than what is being observed experimentally.

4.4 FACS Heating Test of Compact 4-3 at 1000°C

The time-dependent measured and BISON predicted release during the 1000°C FACS isothermal heating test of Compact 4-3 is summarized in Figure 26. The FACS furnace was held at temperature for approximately 300 hours, and the resulting release at the end of the FACS heating test is summarized in Table 14.

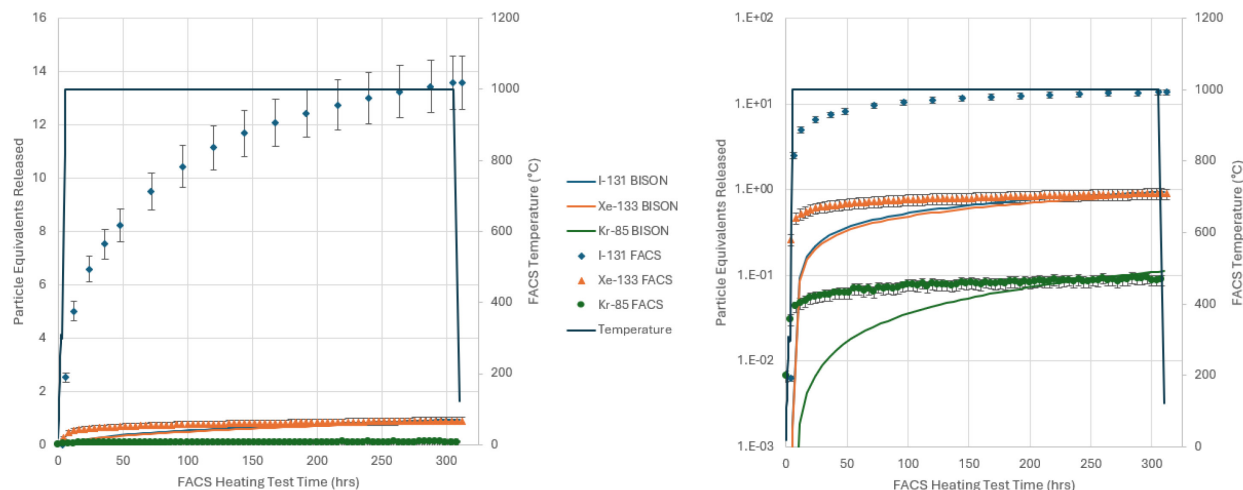


Figure 26. Time-dependent measured release from Compact 4-3 at 1000°C. The same data are plotted on linear (left) and log (right) scales.

Table 14. Total release from Compact 4-3 at 1000°C.

Nuclide	Particle Equivalents		Relative Error
	Measured	BISON	
I-131	13.63	0.95	-93%
Xe-133	0.89	0.87	-2%
Kr-85	0.09	0.11	28%

The measured ^{131}I release is surprisingly high considering Compact 4-3 was the lowest heating test temperature of the four compacts. Even more confounding is that the ^{131}I measured release was over fifteen times higher than the ^{133}Xe measured release when the previous three compacts were on the same order of magnitude. Without any documentation on the measured results from Compact 4-3 to provide context to the ^{131}I release fraction, it is difficult to make any sort of meaningful comparison to the BISON ^{131}I predicted release results. The measured and predicted release results were in fairly good agreement with ^{133}Xe and ^{85}Kr and their total release was the lowest of the four compacts, which was expected since it experienced the lowest isothermal heating test temperature.

4.5 Iodine Release

The measured and BISON predicted time-dependent release of ^{131}I from the four compacts is illustrated in Figure 27. This is the same data presented at the compact level, focused on the individual isotope to further identify trends and discrepancies between the measured and predicted values at the

nuclide level. The ^{131}I total release in terms of DTF inventory fraction is summarized and illustrated in Figure 28.

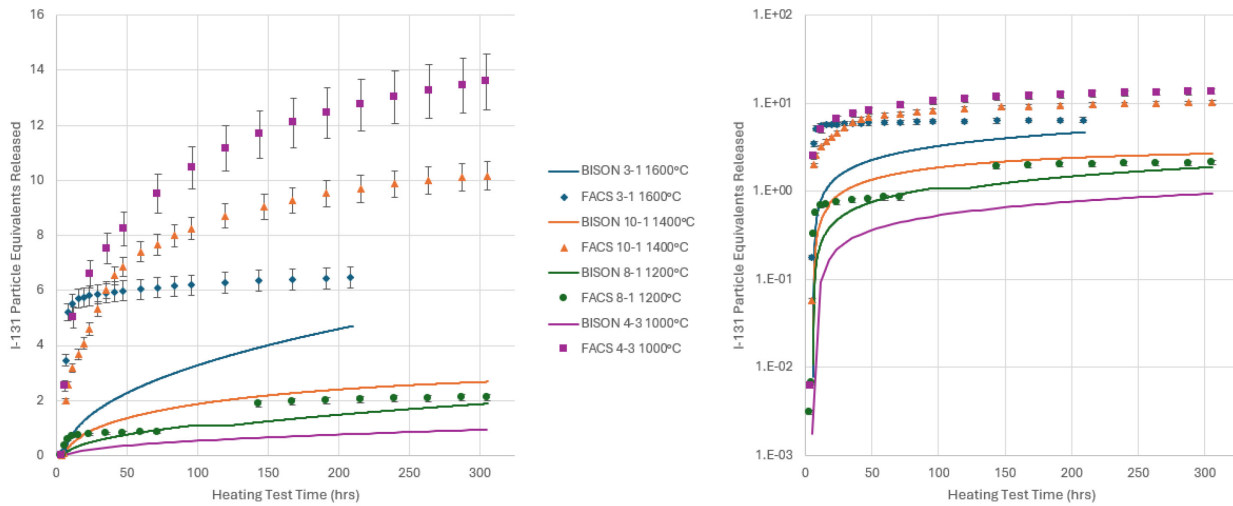


Figure 27. Time-dependent measured release of ^{131}I . The same data are plotted on linear (left) and log (right) scales.

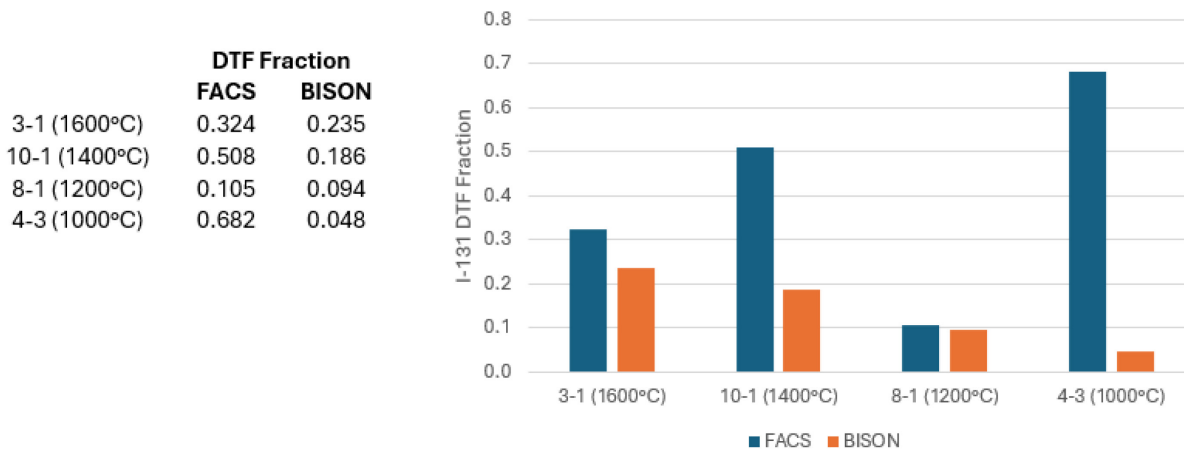


Figure 28. ^{131}I release as a fraction of inventory produced in DTF particles.

With the exception of Compact 8-1, the measured iodine release increases with decreasing FACS heating test temperature. Conversely, the BISON predicted release decreases with decreasing FACS heating test temperature, a fission product release phenomenon that is expected. It is estimated that five percent of the release from Compact 10-1 is from a failed driver fuel particle but even considering this contribution to the measured release, the measured particle equivalents will still be higher than the measured release from Compact 3-1. A comparison of the ^{131}I release early in the FACS heating test between the two compacts is illustrated in Figure 29. At approximately 18 hours, a five percent step change in iodide release from Compact 10-1 can be observed in the BISON results representing the failed driver fuel particle. When comparing the measured results from the two compacts, the iodine release is much faster in Compact 3-1 at the higher FACS temperature early in the test but eventually plateaus at six particle equivalents (eventually reaching 6.47 at the end of the 202-hour test). The iodine release from

Compact 10-1 at 1400°C is much slower but eventually surpasses Compact 3-1 at approximately 36 hours into the heating test. Examining Figure 29 and the release data before 18 hours from Compact 10-1, it is estimated that even without a failed driver fuel particle, the iodine release from Compact 10-1 would eventually surpass Compact 3-1, just later in the FACS heating test. This would suggest that there is an unaccounted-for error in the measured data (either from the measured release or calculated inventory). Capturing and quantifying this measurement error could result in the BISON predictions appearing to perform better than illustrated. As for Compact 4-3, without formal documentation of the measured release results, it is impossible to determine why the iodine release is so high in the compact with the lowest FACS heating test temperature when the BISON predictions suggest it should be much lower.

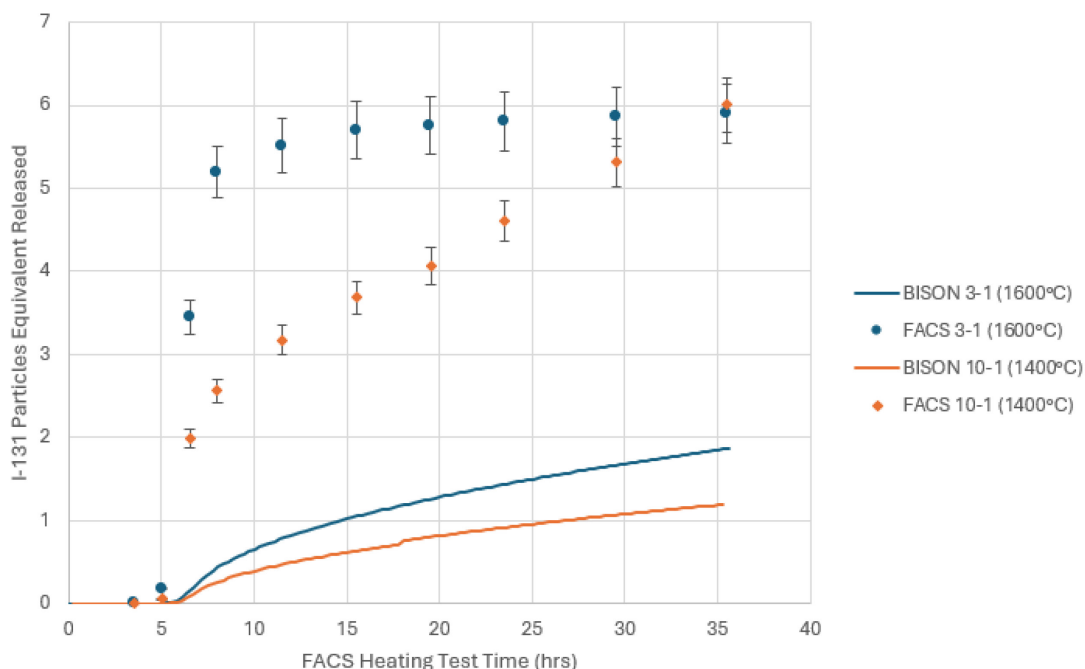


Figure 29. ^{131}I release from Compacts 3-1 and 10-1 early in the FACS heating test.

4.6 Xenon Release

The measured and BISON predicted time-dependent release of ^{133}Xe from the four compacts is illustrated in Figure 30. This is the same data presented at the compact level, focused on the individual isotope to further identify trends and discrepancies between the measured and predicted values at the nuclide level. The ^{133}Xe total release in terms of DTF inventory fraction is summarized and illustrated in Figure 31.

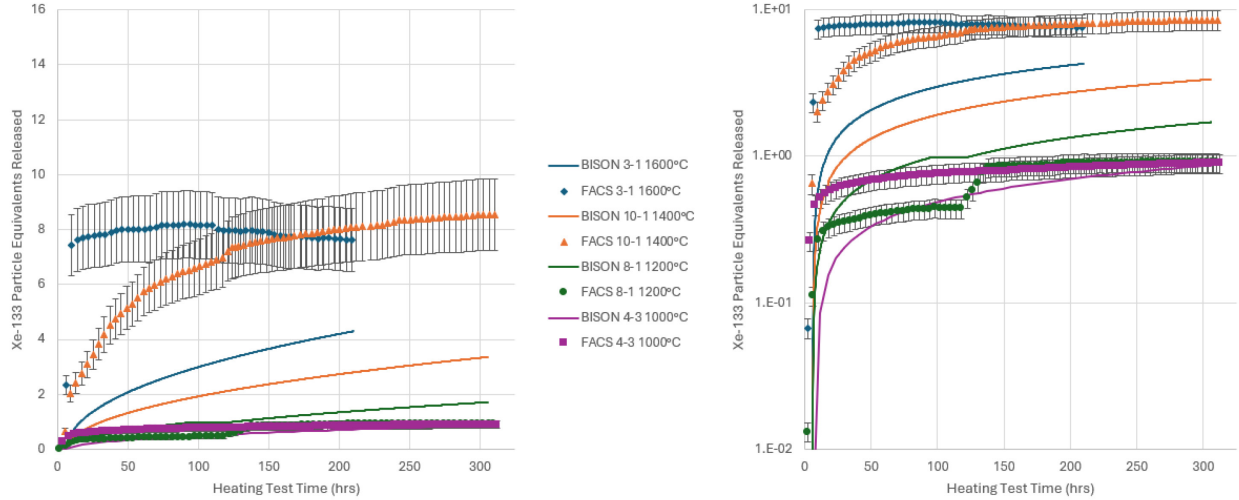


Figure 30. Time-dependent measured release of ^{133}Xe . The same data are plotted on linear (left) and log (right) scales.

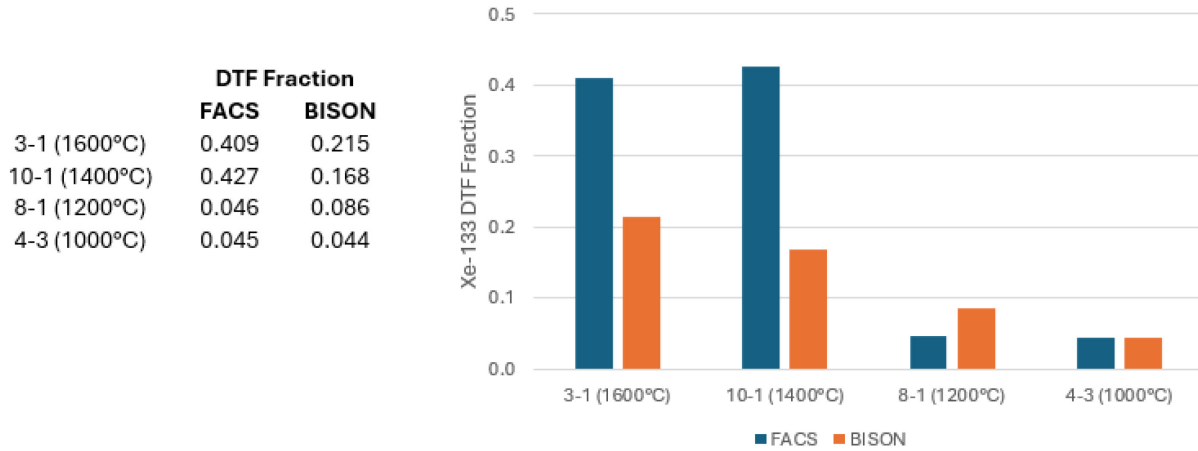


Figure 31. ^{133}Xe release as a fraction of inventory produced in DTF particles.

Again, since the ^{133}Xe measured release decreases in Compact 3-1, the maximum value during the FACS heating test evolution is used to determine the total measured release in terms of particle equivalents as well as to determine the DTF fraction. As a collective, no discernable trends can be identified from the measured release from the four compacts. The two high FACS temperature compacts released similar DTF fractions (0.409 and 0.427 for Compacts 3-1 and 10-1, respectively) and the two lower FACS temperature compacts released similar DTF fractions (0.046 and 0.045 for Compacts 8-1 and 4-3, respectively). This would suggest that ^{133}Xe transport is reduced between 1200°C and 1400°C. However, when compared to the ^{131}I and ^{85}Kr measured results (which assumes the same diffusion coefficients) this phenomenon does not occur, suggesting that xenon specific effective diffusion coefficients should be developed and applied in the models or that there is an unaccounted-for uncertainty in the experimental measurements.

4.7 Krypton Release

Unlike ^{131}I and ^{133}Xe , krypton release is dependent on the inventory at the EOI in the ATR due to the longer half-life and negligible production in NRAD compared to the ATR. The inventory as calculated by

as-run neutronic calculations in the ATR at the EOI plus one day (Sterbentz 2015) and BISON predicted ^{85}Kr inventory (accounting for retention, release, and decay) is illustrated in Figure 32. In general, BISON consistently underpredicts the ^{85}Kr inventory by approximately 27.5%. Since fractional release is used in this study, this difference does not impact the overall comparative analysis since the amount released would also decrease by the same percentage resulting in the same M/C ratio. What is important is the predicted amount of ^{85}Kr remaining in the DTF particles that is available for release during the heating tests. Table 15 summarizes the BISON predicted ^{85}Kr production and retention in the DTF particles along with the fraction available for release at the end of the ATR irradiation. From these predicted results, the diffusivities are low enough that roughly 65% of the ^{85}Kr produced in the DTF particle remains in the compact at the ATR irradiation temperatures. Since the experimental calculated inventory is only provided in snapshots at the EOI in the ATR, EOI in NRAD, and before and after the FACS heating tests and the release (inventory) cannot be distinguished between driver and DTF particles, it is difficult to make any sort of definitive conclusions on how well the BISON predicted ^{85}Kr source term compares to the as-run neutronic calculations.

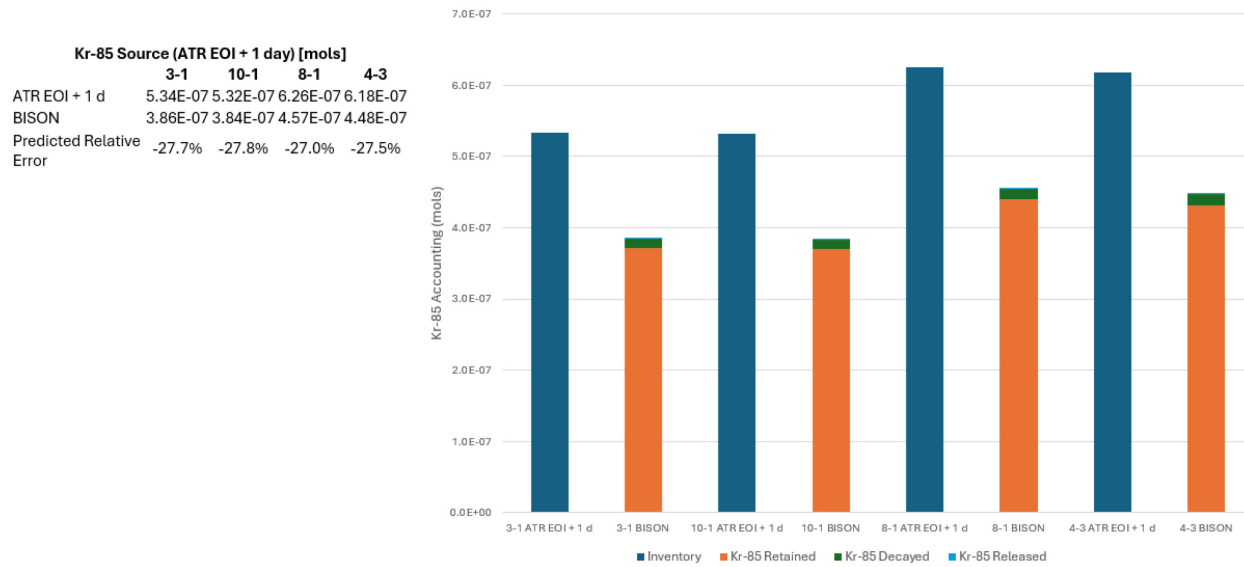


Figure 32. As-run neutronic calculated and BISON predicted ^{85}Kr inventory post ATR irradiation (EOI plus one day).

Table 15. BISON predicted produced and retained ^{85}Kr inventory at the EOI in the ATR.

Compact	ATR TAVA Temperature (°C)	DTF ^{85}Kr Produced (mols)	DTF ^{85}Kr Retained (mols)	DTF Fraction Remaining
3-1	1138	3.97E-09	2.68E-09	68%
10-1	1172	3.95E-09	2.46E-09	62%
8-1	1165	4.70E-09	2.72E-09	58%
4-3	1035	4.61E-09	3.25E-09	70%

The measured and BISON predicted time-dependent release of ^{85}Kr from the four compacts is illustrated in Figure 33. This is the same data presented at the compact level, focused on the individual isotope to further identify trends and discrepancies between the measured and predicted values at the

nuclide level. The ^{85}Kr total release in terms of DTF inventory fraction is summarized and illustrated in Figure 34.

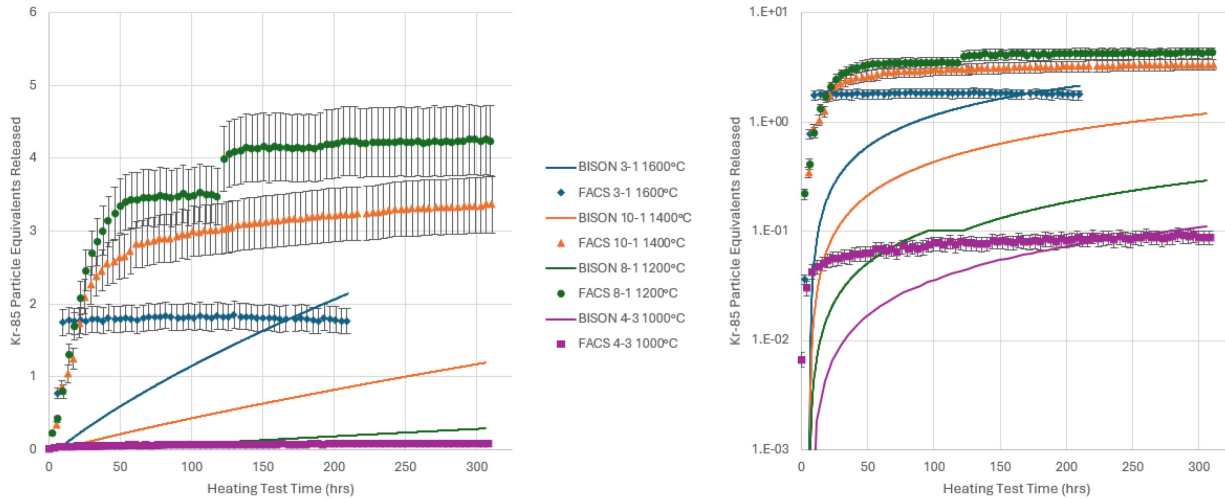


Figure 33. Time-dependent measured release of ^{85}Kr . The same data are plotted on linear (left) and log (right) scales.

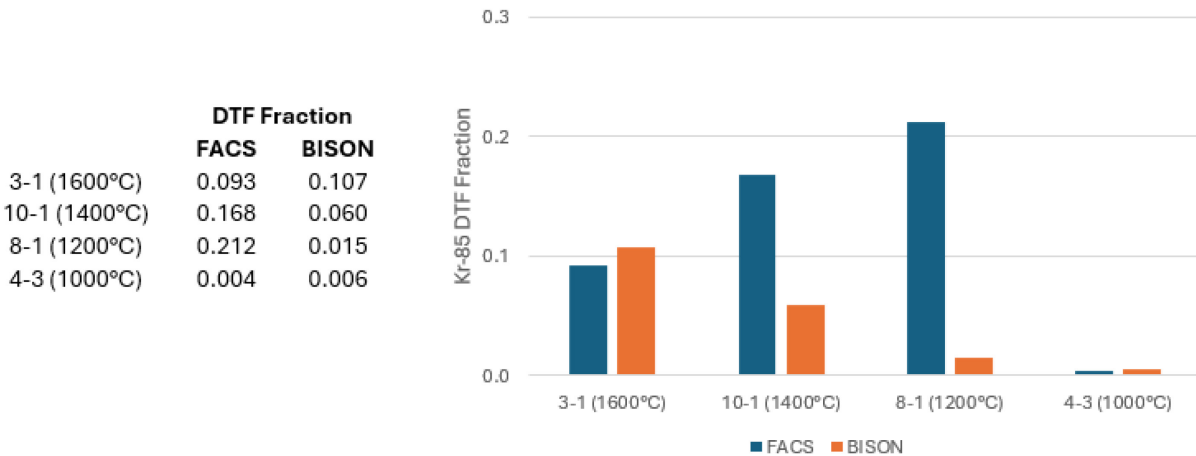


Figure 34. ^{85}Kr release as a fraction of inventory produced in DTF particles.

The measured ^{85}Kr total release increases with decreasing FACS temperatures for three compacts published in (Stempien et al. 2021) whereas the BISON results decrease with decreasing temperature as expected following the application of the Arrhenius diffusion equation. Unlike the short-lived fission products ^{131}I and ^{133}Xe , the fission product inventory of ^{85}Kr is produced during the ATR irradiation, as opposed to the NRAD re-irradiation. As a result, the experimental fission product accounting (decay, release, and production) and the BISON accounting of ^{85}Kr needs additional evaluation to quantify the inventory to properly assess any predicted release results from the BISON simulation. This includes assessing the applicability of the fission product diffusivities used throughout the evolution of the ATR irradiation and subsequent FACS heating test to better inform the BISON simulation and its ability to accurately track fission products.

Figure 33 shows that there is fairly good agreement between the final experimental ^{85}Kr measured release and the BISON predicted release at 1000°C and 1600°C. This is misleading because the starting

condition of the DTF particles is different at the beginning of the FACS heating tests. It is expected that experimental ^{85}Kr inventories in DTF particles are nearly depleted while Table 15 shows that BISON predicts roughly 70% of ^{85}Kr remains in the DTF particle in these two compacts. Further, visual examination of the time-dependent release curves in Figure 33 show a gradual increase of the predicted release of the predicted inventory available in the DTF particles. Although the release fractions agree at the end of the FACS heating test, if allowed to continue, the predicted release would continue to increase while the measured release had reached its plateau. This concludes that the close comparison results were coincidental at the end of the FACS heating tests at these two temperatures. This highlights the underestimation of kernel diffusivities used in BISON that underpredicts krypton release resulting in substantially increased DTF inventories and emphasizes the importance of ensuring the same initial state is used to prevent mischaracterizing predicted results.

5. DISCUSSION OF RESULTS

Performing the entire experiment evolution of ATR irradiation, NRAD re-irradiation, and FACS heating tests to acquire the measured total release values relied on data supplied from ATR thermal evaluations, ATR physics data, NRAD physics data, and collection plate efficiencies (for ^{131}I). Although the measured release uncertainty is illustrated in the figures above (ranging from 5 to 15%), it does not take into consideration the uncertainty in the data provided (ATR nuclide inventory, NRAD nuclide inventory, collection plate efficiency, etc.) to obtain the fractional release and only represents the uncertainty from the actual measurement values that were attained using either condensation collection plates or the FACS FGMS. From the BISON modeling perspective, there were a number of assumptions made (application of UO_2 diffusivities to UCO, spatial temperature distribution, and applying the same diffusivities for all three radionuclides) that could have a substantial impact on the predicted release. The impacts on the unaccounted-for uncertainties in both the measured and predicted values presented is further discussed and analyzed in this section.

Recall that the fractional release compared in this study (in terms of particle equivalents) is a ratio of the experiment measured or BISON predicted release (M_E or M_B , respectively) to the experiment calculated or BISON predicted inventory (C_E or C_B , respectively). Uncertainties in each one of these terms can have a substantial impact on the evaluation between total measured and predicted fractional release if any one of them differ by an order of magnitude.

First, the potential uncertainties from the experimental measured release values are examined (M_E) that are not fully quantified. The collection plate efficiency for ^{131}I has a considerable impact on the final result and can range between 0.1 and 0.47 depending on the temperature of the FACS heating test (Table 2). If collection efficiency is over or underrepresented, the final ^{131}I measured release data will be under or over reported. The uncertainty of the condensation plate efficiencies is not quantified and considered in the ^{131}I measured uncertainties in the data presented above. As for measurement data collected for ^{133}Xe and ^{85}Kr , unaccounted for variables acquiring the measurement data are not considered. One such example is relocation of the noble gas in the charcoal-filled cryotrap which can influence the total measured release, and its impact is not fully quantified. It appears that this occurred in the case of Compact 3-1, for example, causing the accumulated measured release to slightly decrease during the FACS heating test after reaching a maximum value. The maximum values from the two radionuclides were used to compare to the BISON predicted results. In actuality, referring to Figure 22, the total measured particle equivalents released was probably higher than the reported values for ^{133}Xe and ^{85}Kr (8.18 and 1.85 particle equivalents, respectively) which results in an even greater BISON underprediction of ^{133}Xe and less of an overprediction of ^{85}Kr than reported. These uncertainties are not captured in the reported measured results, so it is difficult to gain any meaningful observations when comparing the differences between the measured and BISON predicted results for this compact.

Next, the uncertainties associated with the calculated nuclide inventory uncertainties are examined. It is important to remember that the short-lived fission product inventories are calculated from NRAD

physics calculations and decay-corrected to the start of the FACS heating test and ^{85}Kr calculated inventory is accumulated during the ATR irradiation and decay-corrected to the start of the FACS heating test. The inventory from the physics calculations (C_E) used to calculate the measured fractional release was examined further to help provide insights into the comparisons between measured and BISON predicted results. It was observed that the short-lived fission product inventories determined by the physics calculations at the start of the FACS heating tests differ than what would be expected from a simple decay calculation used in the BISON methodology ($A = A_0 e^{-\lambda t}$). To provide an example, the experiment calculated inventories using both as-run physics calculations and simple decay calculations implemented by BISON are summarized in Table 16 for Compact 3-1 for the short-lived fission products.

Table 16. Physics calculated inventories versus decay-corrected inventories and the resulting measured releases for Compact 3-1.

	I-131	Xe-133
Cumulative activity released at FACS Start (Ci)	1.30E-04	4.07E-04
Half-life $t_{1/2}$ (days)	0.00	0.00
NRAD Physics Calculations		
Calculated end of NRAD (Ci)	7.21E-02	1.79E-01
Calculated activity at FACS start (Ci)	3.84E-02	9.54E-02
Release fraction end of FACS	3.37E-03	4.27E-03
Particle equivalents	6.47	8.18
BISON Methodology		
Calculated end of NRAD (Ci)	7.21E-02	1.79E-01
Decay-corrected activity at FACS start ^a (Ci)	3.54E-02	6.03E-02
Decay-corrected release fraction end of FACS	3.66E-03	6.75E-03
Particle equivalents	7.02	12.95

a. Calculated using $A = A_0 e^{-\lambda t}$ where A_0 is the end of NRAD activity, $\lambda = \text{Ln}(2)/t_{1/2}$, $t = 8.23$ days

To provide context to values summarized in Table 16, the calculated inventories for ^{131}I is discussed applying first the physics calculation methodology and then the simple decay calculation methodology. First, it is important to note that the same cumulative release (M_E) was used for both the physics and decay methodology (1.30×10^{-4} Ci) in the fractional release equation. Using the physics calculation methodology, the reported calculated inventory of ^{131}I at the FACS start was 3.84×10^{-2} Ci (C_E) which results in a release fraction of 3.37×10^{-3} , or 6.47 particle equivalents (same value presented in Table 11). Using the BISON methodology, the activity at the end of the NRAD irradiation was reported to be 7.21×10^{-2} Ci and this value was decay-corrected 8.23 days to the start of the FACS heating test resulting in an activity of 3.54×10^{-2} Ci (C_E). From this value, the release fraction was determined to be 3.66×10^{-3} Ci or 7.02 particle equivalents released. This is an 8.5% difference when compared to the physics calculation methodology. Similar results are illustrated for ^{133}Xe where the difference is 58% when compared to the physics calculation methodology. Not accounting for parent decay chains during both the NRAD re-irradiation and storage before the FACS heating tests will contribute to a discrepancy between the as-run physics calculations and the BISON methodology. This analysis highlights the differences that exist in the experimental inventory calculations and BISON predictions that cannot be fully accounted for or explained to accurately compare the measured release to the BISON predicted release results at this time. A more thorough understanding of the assumptions and methodologies used in the NRAD physics calculations to produce an equivalent methodology in BISON is needed to allow for a more rigorous comparative analysis.

Finally, the uncertainties associated with the BISON predicted results are examined to provide further context between the differences in the measured and predicted release results. First, the BISON release

results are highly dependent on the fission product diffusivities applied throughout the evolution of simulating the ATR irradiation, NRAD re-irradiation, and FACS heating test. BISON relies on these diffusivities to predict fission product release during the ATR irradiation which ultimately correlates to the inventory available for release of long-lived fission products. To further complicate the BISON predicted release and BISON calculated inventory uncertainties is the temperature-dependent fission product diffusivities and the spatial temperature distribution in an irradiated compact, which can vary significantly in a capsule as illustrated in Figure 35 (Hawkes 2016), influencing the fission product transport during the ATR irradiation. The ATR temperature spatial distributions in the AGR-3/4 compacts were obtained from the as-run thermal analysis (Hawkes 2016) and although it uses a large number of thermal nodes (roughly one node per particle) and the BISON simulations account for the spatial distributions of temperature within compact, the discrepancies observed between calculated and measured values when comparing the fractional release could be attributed to an unaccounted for distribution of temperatures. The wide range of temperatures span hundreds of degrees that result in a broad range of diffusivities that introduce another uncertainty in the BISON simulation.

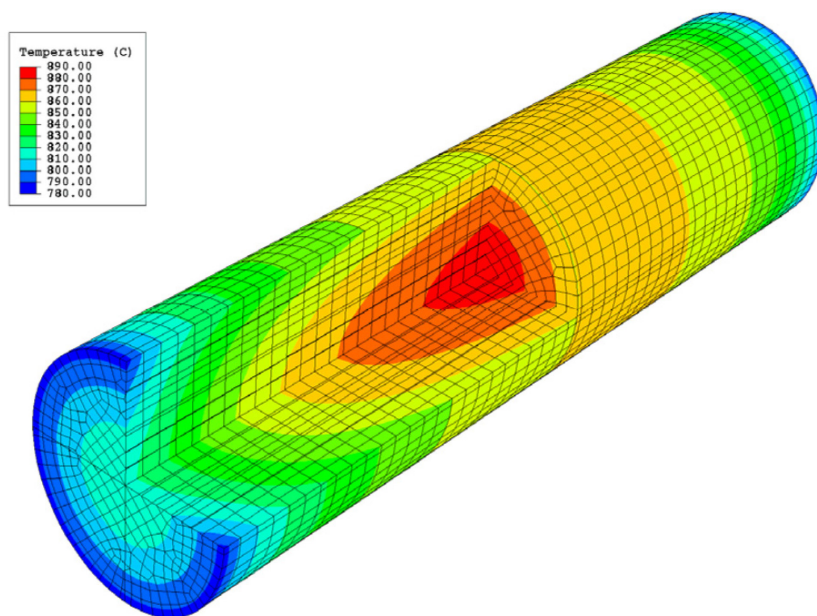


Figure 35. Cut-away view a typical temperature (°C) contour plot of an AGR-3/4 capsule (Hawkes 2016).

As for the short-lived fission products, it is assumed that the compacts were exposed to such a low temperature during the NRAD re-irradiation that no fission product release is expected and all fission products produced during the re-irradiation remains in the particle and are available for release during the FACS heating test. Assuming that this assumption is correct, it is theoretically possible to obtain effective diffusion coefficients for a UCO kernel using BISON for the short-lived isotopes if the fission product inventories are correctly accounted for and the FACS measured release values are fully quantified and assessed such that the BISON models can be properly updated to perform further analyses. For example, the current measured release is inversely proportional to the temperature and an attempt to fit diffusivities to those results would produce fission product transport behavior opposite of that known from solid-state diffusion behavior.

Since it is assumed that all release from the FACS heating test is observed from DTF particles, the kernel diffusivities are extremely important for the BISON predictions. It has already been discussed that diffusivities used in the model were developed using UO_2 fuel and based on the results presented in this report, UCO specific diffusivities should be developed and applied to more accurately predict the release

of ^{131}I , ^{133}Xe , and ^{85}Kr . Even more specific, it may be appropriate to develop element specific UCO kernel diffusivities instead of applying the same kernel diffusivities for all three elements considered in this study.

Generally, based on the results presented in this study, the current kernel diffusivities used in the BISON simulation appear to underpredict the total release fraction. This is supported by visually inspecting the time-dependent fission product release curves for the individual compacts. The BISON predicted time-dependent release takes longer and, in most cases, never reach a cumulative release fraction “plateau” within the heating test time period when compared to the measured results, which can reach this “plateau” shortly after achieving the target heating test temperature. This implies that the BISON release rates are much lower indicating that the kernel diffusivities used in study should be higher. Unfortunately, the UO_2 developed diffusivities used in this study are currently the best estimates available and it is difficult to quantify and assess the impact they have on the BISON simulation globally since they are used throughout the evolution of this process. Ideally, BISON fission product tracking results would be evaluated incrementally at each compact evolution step (ATR irradiation, NRAD re-irradiation, and the subsequent FACS heating test) and the predicted fission product inventories would be compared to experimentally measured values obtained before and after each evolution. This would be a much more informed approach to assess and quantify the errors and uncertainties associated with fission product diffusivities and ultimately the impact they have on both the measured BISON release (M_B) and BISON calculated inventory (C_B).

6. CONCLUSION

Currently, BISON includes source term models for elemental Ag, Cs, Sr, Kr, and Xe, which were originally obtained from PARFUME. These models were not suitable for the current work, which focused on tracking the production, decay, transport, and release of three specific radionuclides within and from fueled compacts: ^{131}I , ^{133}Xe , and ^{85}Kr . As such, significant model development involving both BISON and Griffin/DRAGON was needed to enable these analyses. Simplified multigroup cross-sections were prepared for the AGR-2 experiment conducted in ATR using DRAGON and applied to model composition evolution within the fuel using Griffin. These predictions were compared to previous AGR calculations with reasonably favorable results, building confidence for their development into preliminary nuclide-specific source term models for BISON. These proof-of-concept models were combined with limited transport data from the literature—recall that one kernel diffusivity was available and applied to all three radionuclides—to model radionuclide conservation during the AGR-3/4 experiment in ATR and subsequent re-irradiation in NRAD and high-temperature testing in FACS.

Using this newly developed specific fission product tracking methodology, BISON was used to predict the fission product release fraction of ^{131}I , ^{133}Xe , and ^{85}Kr from four AGR-3/4 re-irradiated fuel compacts during their respective heating tests. These compacts were subjected to a 369.1 EFPD ATR irradiation, storage, approximately five-day NRAD re-irradiation, storage, and finally heated in the INL FACS furnace between 200 to 300 hours. Model predictions were then compared to the measured fission product release fractions for these radionuclides during heating tests in the FACS furnace at INL. These isothermal heating tests were conducted at target temperatures between 1000°C and 1600°C.

Although comparative results varied in this study at the compact-level and at the individual radionuclide level from the different FACS target temperatures the following observations are made:

- The BISON predicted total release results decrease with decreasing FACS temperatures, a phenomenon that is consistent with the application of the temperature-dependent Arrhenius diffusion equation. The experimental measured release results on the other hand, were frequently inversely proportional to FACS test temperature. Notably, ^{131}I release observed at 1000°C was more than twice that observed at 1600°C. This highlights the substantial difficulties associated with this type of testing, which can be influenced by uncertainties in irradiation and re-irradiation conditions, furnace detector efficiencies, unexpected particle failures, and more.

- The BISON predicted fractional release, in terms of particle equivalents, agreed within about 0–4 particle equivalents at 1600°C, 2–6 particle equivalents at 1400°C, 0–4 particle equivalents at 1200°C, and 0–12 particle equivalents at 1000°C.
- In general, BISON results underpredict the total DTF release of the three fission products, suggesting that the fuel kernel effective diffusion coefficients used in BISON are too low. This is supported by the visual inspection of the time-dependent release results indicating lower release rates predicted by BISON.
- Assuming the release of the short-lived fission products generated from the NRAD re-irradiation are from DTF fuel particles, it is possible to use BISON to develop UCO specific effective diffusion coefficients for ^{131}I and ^{133}Xe with a more rigorous analysis of experimental data, spatial temperature distribution, and BISON predicted release behavior.

As this report shows, validating fission product transport is difficult due to the complexities of the experiments and their associated uncertainties. Model predictions (both as-run physics calculations and BISON simulations) of re-irradiated AGR-3/4 compacts are dependent on how well the codes account for the fission product inventories in intact drive fuel particles and DTF particles during the ATR irradiation (^{85}Kr) and NRAD irradiation (^{131}I and ^{133}Xe) prior to performing the FACS heating test. There is also uncertainty in the source of fission products released during the heating tests, since only the cumulative compact release is measured, and this can complicate comparison with the models.

Admittedly, the level of agreement in this comparative analysis is not ideal, and for now, it may preclude the possibility of inferring more accurate diffusivities for the nuclides of interest. Taken as a whole, however, these results are considered promising because (1) the release predictions exhibit the expected physical behavior with respect to temperature and (2) the comparisons are favorable if the inconsistencies in the measured releases with respect to temperature are interpreted as noise or some other behavior that the models cannot yet account for.

Given the substantial overhead associated with performing these experimental tests, it may be impractical to collect enough measurements in the short-term to fully investigate and characterize the source of the unexpected thermal behaviors. Within that context, it may be reasonable to use these measurements and comparisons to establish bands for the number of particles that can confidently be said to have failed based on radionuclide release from a given compact. In the meantime, the authors recommend further development of the preliminary source term models, more detailed comparisons with existing AGR composition calculations, incorporation of additional diffusivity data as it becomes available, and perhaps full multiphysics analyses (depletion and transmutation plus fuel performance) of the experiments to help reduce uncertainties in the simulation predictions.

7. REFERENCES

- Barnes, C. M. 2006a. *AGR-1 Fuel Product Specification and Characterization Guidance*. EDF-4380, Rev. 8, Idaho National Laboratory.
- Barnes, C. M. 2006b. *AGR-3 & 4 Fuel Product Specification*. EDF-6638, Rev. 1, Idaho National Laboratory.
- Bess, J. D., J. B. Briggs, R. M. Lell. 2014 *Neutron Radiography (NRAD) Reactor 64-Element Core Upgrade*. INL/EXT-13-29628, Rev. 0, Idaho National Laboratory.
<https://doi.org/10.2172/1120810>.
- BWXT. 2006. *Industrial Fuel Fabrication and Development Lot G73V-20-69303*. Data Certification Package, BWX Technologies.

- CEGA. 1993. *NP-MHTGR Material Models of Pyrocarbon and Pyrolytic Silicon Carbide*. CEGA-002820, Rev. 1, CEGA Corporation.
- Collin, B. P., 2014, *Comparison of Fission Product Release Predictions Using PARFUME with Results from the AGR-1 Safety Test*. INL/EXT-14-31976, Rev. 0, Idaho National Laboratory. <https://doi.org/10.2172/1164853>.
- Collin, B. P., 2016. *AGR-3/4 Irradiation Test Final As-Run Report*. INL/EXT-15-35550, Rev. 1, Idaho National Laboratory. <https://doi.org/10.2172/1468992>.
- Collin, B. P. 2018. *AGR-2 Irradiation Test Final As-Run Report*. INL/EXT-14-32277, Rev. 4, Idaho National Laboratory. <https://doi.org/10.2172/1514716>.
- Demkowicz, P. A. 2017. *AGR-3/4 Phase 2 Post-Irradiation Examination Plan*. PLN-5382, Rev. 0, Idaho National Laboratory.
- Demkowicz, P. A., D. V. Laug, D. M. Scates, E. L. Reber, L. G. Roybal, J. B. Walter, J. M. Harp, and R. N. Morris. 2012. "The Fuel Accident Condition Simulator (FACS) furnace system for high temperature performance testing of VHTR fuel." *Nuclear Engineering Design* 251: 164-172. <https://doi.org/10.1016/j.nucengdes.2011.10.048>.
- Demkowicz, P. A., E. L. Reber, D. M. Scates, L. Scott, and B. P. Collin 2015. "First high temperature safety tests of AGR-1 TRISO fuel with the Fuel Accident Condition Simulator (FACS) furnace." *Journal of Nuclear Materials* 464: 320-330. <https://doi.org/10.1016/j.jnucmat.2015.05.006>.
- Giudicelli, G., A. Lindsay, L. Harbour, C. Icenhour, M. Li, J. E. Hansel, P. German, P. Behne, et al. 2024. "3.0 MOOSE: Enabling Massively Parallel Multiphysics Simulation." *SoftwareX* 26: 101690. <https://doi.org/10.1016/j.softx.2024.101690>.
- Hales, J. D., W. Jiang, A. Toptan, and K. A. Gamble. 2020. *BISON TRISO Modeling Advancements and Validation to AGR-1 Data*. INL/EXT-20-59368, Rev. 0, Idaho National Laboratory. <https://doi.org/10.2172/1711423>.
- Hales, J. D., A. Toptan, W. Jiang, and B. W. Spencer. 2021a. "Numerical Evaluation of AGR-2 Fission Product Release." *Journal of Nuclear Materials* 558: 153325. <https://doi.org/10.1016/j.jnucmat.2021.153325>.
- Hales, J. D., W. Jiang, A. Toptan, and K. A. Gamble. 2021b. "Modeling Fission Product Diffusion in TRISO Fuel Particles in BISON." *Journal of Nuclear Materials* 548: 152840. <https://doi.org/10.1016/j.jnucmat.2021.152840>.
- Hawkes, G. L. 2014. *AGR-2 Daily As-Run Thermal Analyses*. ECAR-2476, Rev. 1, Idaho National Laboratory.
- Hawkes, G. L. 2016. *AGR-3/4 Daily As-Run Thermal Analyses*. ECAR-2807, Rev. 1, Idaho National Laboratory.
- Hull, L., M. Plummer, N. Johnson. 2020. *NDMAS System and Process Description*. INL/EXT-12-27594, Rev. 2, Idaho National Laboratory <https://www.osti.gov/servlets/purl/1615632>.
- Hunn, J. D., and R. A. Lowden. 2007, *Data Compilation for AGR-3/4 Driver Fuel Coated Particle Composite LEU03-09T*. ORNL/TM-2007/019, Oak Ridge National Laboratory. <https://doi.org/10.2172/931362>.
- IAEA. 1997. *Fuel Performance and Fission Product Behaviour in Gas Cooled Reactors*. IAEA-TECDOC-978, International Atomic Energy Agency.
- Jiang, W., G. Singh, J. D. Hales, A. Toptan, B. W. Spencer, S. R. Novascone, S. L.N. Dhulipala, and Z. M. Prince. 2022. "Efficient High-fidelity TRISO Statistical Failure Analysis using BISON:

- Applications to AGR-2 Irradiation Testing." *Journal of Nuclear Materials* 562: 153585. <https://doi.org/10.1016/j.jnucmat.2022.153585>.
- Jiang, W., J. D. Hales, B. W. Spencer, B. P. Collin, A. E. Slaughter, S. R. Novascone, A. Toptan, et al. 2021. "TRISO Particle Fuel Performance and Failure Analysis with BISON." *Journal of Nuclear Materials* 548: 152795. <https://doi.org/10.1016/j.jnucmat.2021.152795>.
- Kercher, A. K., B. C. Jolly, F. C. Montgomery, C. M. Silva, and J. D. Hunn. 2011. *Data Compilation for AGR-3/4 Designed-To-Fail (DTF) Fuel Particle Batch LEU03-07DTF*. ORNL/TM-2011/109, Oak Ridge National Laboratory. <https://doi.org/10.2172/1649083>
- Maki, J. T. 2011. *AGR-3/4 Irradiation Test Specification*. SPC-1345, Rev. 0, Idaho National Laboratory.
- Marleau, G., A. Hébert, and R. Roy. 2024. *A User Guide for DRAGON Version5*. Technical Report IGE-335, École Polytechnique de Montréal. <http://merlin.polymtl.ca/downloads/IGE335.pdf>.
- Marshall, D. W. 2011. *AGR-3/4 DTF Fuel and Capsule Component Material Specifications*. SPC-1214, Rev. 1, Idaho National Laboratory.
- Miller, G. K., D. A. Petti, J. T. Maki, D. L. Knudson, and W. F. Skerjanc. 2023. *PARFUME Theory and Model Basis Report*. INL/EXT-08-14497, Rev. 2, Idaho National Laboratory. <https://doi.org/10.2172/1471713>.
- Mitchell, T. R., and P. A. Demkowicz 2022. *Technical Program Plan for INL Advanced Reactor Technologies Advanced Reactor Fuel Development and Qualification Program*. PLN-3636, Rev. 11, Idaho National Laboratory.
- Skerjanc, W. F. 2020. *Comparison of Fission Product Release Predictions using PARFUME with Results from the AGR-2 Irradiation Experiment*. INL/EXT-20-59448, Rev. 0, Idaho National Laboratory, <https://www.osti.gov/biblio/1688794>.
- Skerjanc, W. F. 2023. *PARFUME/BISON Fission Product Release Predictions versus AGR-3/4 Heating Test Measurements*. INL/RPT-23-74505, Rev. 0, Idaho National Laboratory. <https://www.osti.gov/biblio/2000032>.
- Stempien, J. D, P. A Demkowicz, E. L. Reber, and C. L. Christensen 2018. "Preliminary results from the first round of post irradiation heating tests of fuel compacts from the AGR 3/4 irradiation." Proceedings of HTR 2018, HTR 2018-3023. <https://www.osti.gov/biblio/1478513>.
- Stempien, J. D., P. A. Demkowicz, E. L. Reber, and C. L. Christensen. 2021. "Reirradiation and Heating Testing of AGR-3/4 TRISO Fuels." Proceedings of HTR 2021. HTR 2021-3004.
- Sterbentz, J. W. 2014. *JMOCUP As-Run Daily Depletion Calculation for the AGR-2 Experiment in the ATR B-12 Position*. ECAR-2066, Rev. 2, Idaho National Laboratory.
- Sterbentz, J. W. 2015. *JMOCUP As-Run Daily Physics Depletion Calculation for the AGR-3/4 TRISO Particle Experiment in ATR Northeast Flux Trap*. ECAR-2753, Rev. 1, Idaho National Laboratory.
- Wang, Y., Z. M. Prince, O. W. Calvin, H. Park, N. Choi, Y. S. Jung, S. Schunerta, S. Kumar, J. T. Hanophy, V. M. Labouré, C. Lee, J. Ortensi, L. H. Harbour, J. R. Harter. 2024, "Griffin: a MOOSE-based reactor physics application for multiphysics simulation of advanced nuclear reactors." *Annals of Nuclear Energy* Pre-print. <https://doi.org/10.2139/ssrn.4844473>.
- Williamson, R. L., J. D. Hales, S. R. Novascone, G. Pastore, K. A. Gamble, B. W. Spencer, W. Jiang, et al. 2021. "BISON: A Flexible Code for Advanced Simulation of the Performance of Multiple Nuclear Fuel Forms." *Nuclear Technology* 207 (7): 954 - 980. <https://doi.org/10.1080/00295450.2020.1836940>.